CHALMERS
UNIVERSITY OF TECHNOLOGY

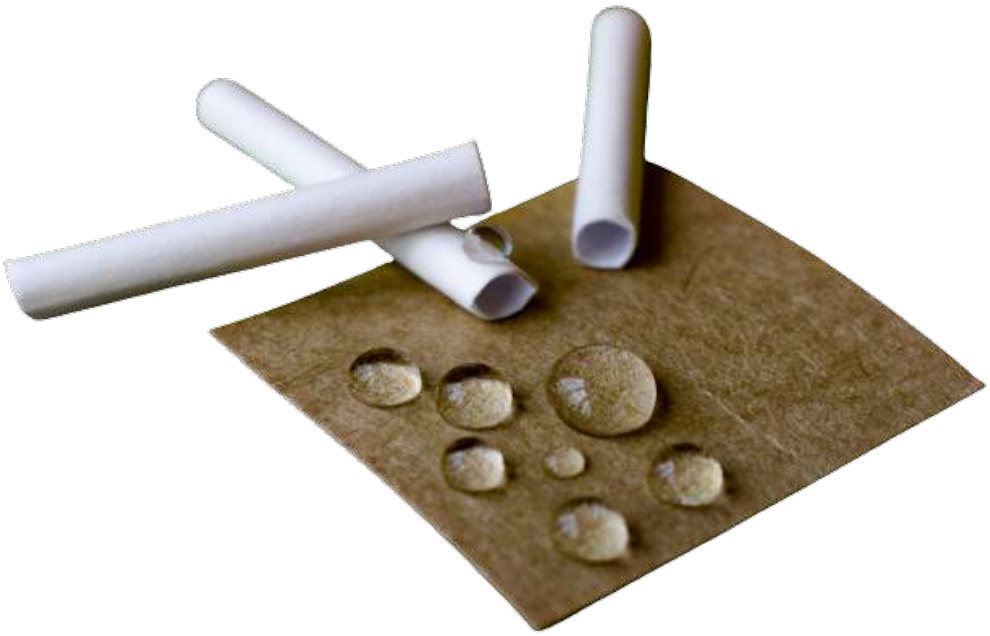

# Experimental Method Development for MRI Moisture Measurements in Paper Materials

STUART HOBSON, NIKETH VENKATESH

DEPARTMENT OF CHEMISTRY AND CHEMICAL ENGINEERING
CHALMERS UNIVERSITY OF TECHNOLOGY
Gothenburg, Sweden 2022
www.chalmers.se

Master's thesis 2022

# Experimental Method Development for MRI Moisture Measurements in Paper Materials

STUART HOBSON
NIKETH VENKATESH


CHALMERS
UNIVERSITY OF TECHNOLOGY

DEPARTMENT OF CHEMISTRY AND CHEMICAL ENGINEERING
*Division of Chemical Engineering*
Chalmers University of Technology
Gothenburg, Sweden 2022

Experimental Method Development for MRI
Moisture Measurements in Paper Materials
STUART HOBSON
NIKETH VENKATESH

Supervisor(s): Dr. Eskil Andreasson, Tetra Pak®
Dr. Marcus Alexandersson, Tetra Pak®
Examiner: Associate Professor Diana Bernin, Chalmers University of Technology

Master's Thesis 2022
Department of Chemistry and Chemical Engineering
Division of Chemical Engineering
Chalmers University of Technology
SE-412 96 Gothenburg
Telephone +46 31 772 1000

Cover: Liquid droplets upon sample materials

Typeset in LaTeX
Gothenburg, Sweden 2022

# Abstract

An understanding of moisture transport within sized paperboards is an important quality aspect for the packaging industry. In this study, the experimental technique of magnetic resonance imaging (MRI) is used to develop a testing methodology which can measure, characterise and quantify the transport of water within paper materials.

A methodology for in-plane liquid uptake measurements within the MRI was developed and found to be applicable for hydrophilic materials. Through thickness testing was performed in the MRI and 1-D profiles were obtained along the through-thickness direction of the paper materials with a spatial resolution of 31$\mu$m and a temporal resolution of 2 minutes measurement acquisition time. To give further insight into the mechanisms of liquid transport within the fibre structure of the paper materials apparent diffusion coefficients were estimated and found to be on the order of $10^{-12}$ $m^2/s$ which strongly suggest that the rate defining mechanism for hydrophobized paper is moisture diffusion within the fibers. This study also explores the various issues encountered during method development and lays a foundation for further work.



Keywords: MRI; Paperboard; Moisture diffusion; Through thickness measurement; In-plane measurement

# Acknowledgements

Firstly, we would like to thank our supervisor and examiner with Chalmers University of Technology, Dr. Diana Bernin, for the opportunity to work under her and being enthusiastically open to discuss all questions, thoughts, and ideas we had during the course of this thesis. We would also like to thank our supervisors from Tetra Pak®, Dr. Eskil Andreasson and Dr. Marcus Alexandersson for their constant enthusiasm, guidance, support and advice throughout the process. This project is part of the Vinnova competence centre FibRe.

We would like to thank Emmanouela Leventaki for helping us with the 3-D printing of new parts for our experiments and Dr. Francisco Baena-Moreno for his assistance with material SEM imaging and analysis. We would also like to thank Torbjörn from the workshop for helping make parts under short notice for our experiments.

Finally, we would like to thank the Department of Chemistry and Chemical Engineering at Chalmers, all those who lent a helping hand with experiments and our friends and colleagues for the active discussions and suggestions which helped make this thesis a success.

# List of Acronyms

Below is the list of acronyms that have been used throughout this thesis listed in alphabetical order:

| | |
|---|---|
| AKD | Alkylketene Dimer |
| AOI | Area of Interest |
| ASA | Alkenyl Succinc Anhydrine |
| CD | Cross Direction |
| FOV | Field of View |
| MD | Machine Direction |
| MRI | Magnetic Resonance Imaging |
| MSME | Multiple Slice Multiple Echo |
| NIR | Near Infrared Spectroscopy |
| NMR | Nuclear Magnetic Resonance |
| NSA | Number of Signal Averages |
| RF | Radiofrequency |
| SEM | Scanning Electron Microscope |
| SNR | Signal to Noise Ratio |
| TE | Echo Time |
| TR | Repetition Time |
| ZD | Out-of-plane Direction |

# Nomenclature

Below is the nomenclature that has been used throughout this thesis.

| | |
|---|---|
| $\nu$ | Larmor frequency (MHz) |
| $\gamma$ | Gyromagnetic ratio |
| B | Magnetic field (T) |
| $M_z$ | Longitudinal magnetization |
| $M_{xy}$ | Transverse magnetization |
| T | Tesla |
| z | Distance liquid has travelled through the material (m) |
| D | Diffusion coefficient ($m^2/s$) |
| t | Time to reach reference uptake level (s) |

# Contents

# List of Figures

# List of Tables

# 1
# Introduction

## 1.1 Background

Paper materials are widely used as sustainable packaging, corrugated board, printing paper and product materials in a selection of industries including the food and beverage industry. Paper materials can fulfill the role of an alternative to single-use plastics, notably for single-use applications such as plastic straws. Paper materials consist of cellulose fibres layered as a porous matrix. The fibres separated by interfibral spaces include large and irregular shaped pores [4]. The fibres and the structure absorb water while the pores hold the water in their natural hydrophilic or processed hydrophobic states. The mechanical strength of the paper matrix depends to a large extent on the moisture content of the material [14]. Moisture-material interactions are thus important to monitor and to understand in order to optimise material performance.

For packing materials, in which mechanical strength is an important product quality aspect; the understanding of transport, swelling and mechanical degradation processes are essential in designing improved packaging materials and paper products in the future. Liquid transport and flow problems within cellulose fibre materials have been widely researched and published across various applications and focusing on a variety of aspects. MRI is however a less explored method through which non-invasive measurements can be made in real time within the paper structure itself without the need for the material being transparent. These qualities are a benefit over widely used methods available to measure moisture content, and notably moisture content within thin sheets such as near infared spectroscopy (NIR), terahertz radiation, or radiography methods[19]. The main drawbacks with these methods are that they cannot be adopted for measuring the through thickness profiles with good spatial resolution or that they are costly and not widely available.

## 1.2 Aim

The aim of this work is to develop a methodology to measure the moisture transport in sized paper materials with high spatial and temporal resolution using MRI. This work explores the future applications and possibilities of MRI within the paper industry through developing and assessing methodologies with which to measure, characterise and quantify liquid transport within paper materials to high spatial and temporal resolutions. This knowledge can be used to characterize the paper

materials and the moisture transport which would help guide the development to further introduce novel and innovative paper-based packaging solutions.

# 2

# Magnetic Resonance Imaging

## 2.1 Basic concepts

Magnetic Resonance Imaging (MRI) is a non-destructive and non-invasive imaging methodology that was first applied in the medical field but has recently started developing applications in experimental investigations of moisture in paper samples [7]. This method provides useful information on the material properties and the evolution during processes like absorption or drying with high spatial and temporal resolution [7].

An MRI instrument mainly consists of a magnet, radiofrequency (RF) transmitter and a receiver. It is based on the principles of Nuclear Magnetic Resonance (NMR). An overview of the underlying principles of this method is described below:

- Nuclei that are placed in a magnetic field of strength B, will precess with the frequency $\nu$, which creates a net magnetization. Think of precession as the rotation observed of a spinning top or gyroscope. The frequency also called the Larmor frequency depends on the gyromagnetic ratio $\gamma$ of the spin.

$$\nu = \gamma B \tag{2.1}$$

  The Larmor frequency of the MRI in this study is 300 MHz.
- It is favorable to run NMR/MRI on isotopes whose natural abundance is high for example $^{1}$H because the signal will get larger with more presence since the MRI is very insensitive.
- The net magnetization can be disturbed when applying a RF pulse [14]. The net magnetization will return to the thermal equilibrium. In other words, the RF pulses will excite the protons $^{1}$H in the sample [17].

To get a better understanding of how the nucleus behaves when placed in a magnetic field, let us consider a proton. As we know, each nucleus has some spin property associated with it. When this nucleus is placed in the magnetic field, the magnetization vector aligns itself with the magnetic field and its behavior is similar to that of a magnet with a north and south pole. It has 2 different energy levels that it can transition between. A low energy level, where the poles align in N-S-N-S direction and a high energy level, where the poles align N-N-S-S direction [12]. An illustration of this concept can be seen in Figure 2.1

The process of imaging is as follows:

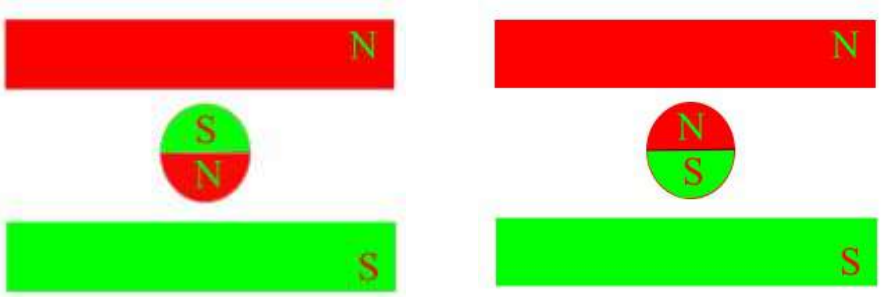


(a) Low energy level (b) High energy level

**Figure 2.1:** Energy levels

- An external RF pulse is introduced to excite the protons in the sample.
- The nuclei return to the thermal equilibrium depending on the "relaxation" process. The signal is recorded as a function of time.
- The raw signal is converted to corresponding intensity levels using a Fourier transform.
- The intensity levels are then displayed as different shades of grey or other colors in a matrix arrangement of pixels.
- The contrast of the images can be varied by changing the sequence of RF pulses applied. Thus different images can be created.

The precession of the protons disturbed back to thermal equilibrium can be visualised through Figure 2.2
.

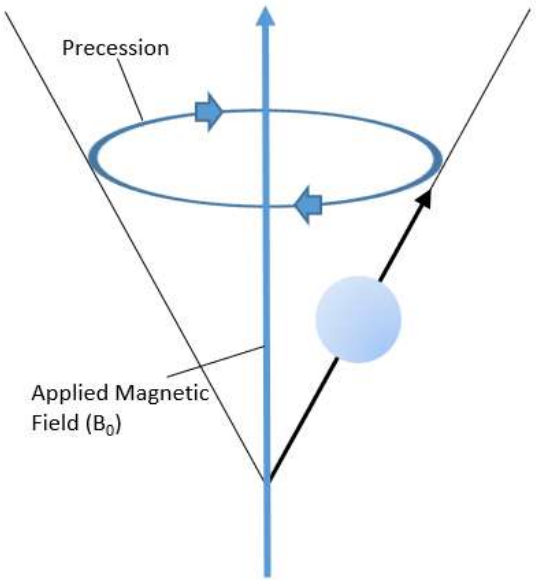


**Figure 2.2:** Precession of proton

There are primarily two controls that are important when determining the contrast. The contrast can be varied by changing these parameters depending on the

type of imaging required.

- **Repetition Time (TR):**It is primarily the time before the first 90 degree RF pulse. A longer TR would allow the protons to relax back to thermal equilibrium while a shorter TR would not have had the protons fully relaxed by the time for the next measure. This would result in a decreasing signal. This phenomenon is related to the T1.
- **Echo Time (TE):**It is primarily the time between the initial 90 degree RF pulse and the echo. A longer echo time would most likely make the protons go out of phase which results in reduced signal while a shorter echo time would reduce the amount of dephasing that can occur. This phenomenon is related to the T2.

## 2.2 Imaging applications

### Relaxation

The most common types of MRI scans are T1-weighted scans and T2-weighted scans. Depending on the type of relaxation (T1 or T2), the signal to noise ratio (SNR) is more or less affected. The T1 relaxation time, also called the spin-lattice relaxation time measures how quickly the excited protons return to equilibrium (or) how the net magnetization vector recovers to its ground level in the direction of the magnetic field [21].

The T2 relaxation time, also called as transverse relaxation time is the rate at which the excited protons reach equilibrium or go out of phase together [22]. Anything causing T1 relaxation causes T2 relaxation also, but T2 relaxation can occur without T1 relaxation too. T2 is always less than or equal to T1. Short echo and repetition times are used to produce T1-weighted images. Alternatively, longer echo and repetition times are used to produce T2-weighted images.

In pure water, the T1 and T2 have comparable magnitude, about 3-4 seconds long [22]. A general illustration of the T1 and T2 relaxation curves can be seen in Figure 2.3

## 2.3 Imaging considerations

MRI is often limited by poor signal to noise ratio and hence optimizing the settings within the MRI is an important step in order to get images and profiles of high spatial and temporal resolution. This is an important part of method development and depends specifically on the type of material tested on and rig setup used. There is a trade off between the taking images with high spatial and temporal resolution but the same needs to be done whilst minimizing the amount of noise. Depending on the scope of the investigation, certain process conditions and physical attributes demand certain considerations with respect to size and rate of process changes.

Before going through the different settings within the MRI, it is important to

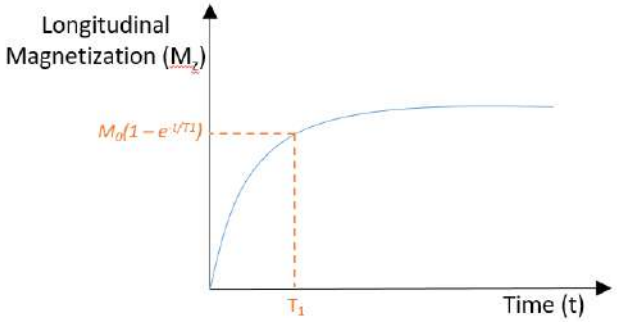


(a) T1 Relaxation

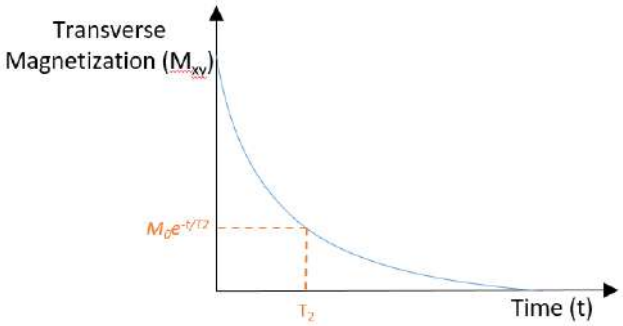


(b) T2 Relaxation

**Figure 2.3:** T1 and T2 Relaxation curves

know what some of the important terms mean and how they are involved in the imaging process. These are summarised below [10] .

### Spatial Resolution:

An MRI image is composed of several voxels. The voxel size is the spatial resolution of the image. It is a 3D unit of the image with a single value, like how pixels are used for representing 2D information [27]. Since voxels are in 3D, the resolution depends on matrix size, field of view (FOV) and slice thickness.

- Resolution is directly proportional to the number of pixels. Pixel size can be calculated by dividing FOV by matrix size.
- Two resolution parameters used in MRI for production of a 2D image are basic resolution and phase resolution.

### Basic resolution:

It determines the size of the image matrix. It is inversely proportional to the pixel size. So, lower resolution means larger pixel size.

### Phase Resolution:

It is the number of pixels in the phase direction. It is normally expressed as a percentage value of the basic resolution. Decreasing the phase resolution will increase

the pixel size in one direction and result in a rectangular pixel shape. Increasing phase resolution will also generally result in a prolonged scan time.

**Signal-To-Noise Ratio (SNR):**

SNR is a standard used to describe the performance of an MRI system. An MRI image is created by a combination of MRI signals and background noise.
MRI image = signal + noise
SNR = signal/noise

**Number of Signal Averages (NSA):**

It is a measurement parameter and is primarily used to improve the SNR. Doubling the NSA improves the SNR by a factor of $\sqrt{2}$ because random noise is also sampled. Thus, as NSA increases, noise begins to get cancelled out. Repeated sampling and the accumulation of signal results in a high signal image, but the drawback is that increasing the NSA also increases the scan time significantly which hence affects the temporal resolution.

The most common settings that are usually optimised within the MRI are Resolution, Repetition Time, Echo Time, Slice Thickness, Field of View and NSA. All of these directly or indirectly affect the SNR of the image obtained. They are also changed depending on the type and contrast of image required. Some of their effects on the SNR are summarised below

**Basic Resolution and SNR**
SNR is inversely proportional to basic resolution. Hence it is directly proportional to pixel size. Increasing the base resolution will reduce the pixel size and therefore the SNR of the image will be reduced.
Increasing the basic resolution will increase the image quality but increasing it more than the acceptable range will produce grainy images due to low SNR and reducing it below the acceptable range will produce blurry images due to high SNR.

**Phase Resolution and SNR**
Decreasing the phase resolution will reduce the image quality and scan time. Reducing phase resolution will increase the pixel size and thus the SNR will decrease.

**TR and SNR**
Increasing TR will increase the SNR since a high TR will allow the longitudinal magnetization to approach its maximum and produce high signal intensities. But increasing the TR beyond a certain limit will reduce the T1 effect.

**TE and SNR**
Increasing the TE will reduce the SNR. A long TE will cause the transverse magnetisation to decay to very low values and result in signal loss. Decreasing the TE beyond a certain limit will reduce the T2 effect. Reduction of TE to increase the SNR should only be used for T1 weighted sequences as that reduces the effect of

T2.

**Slice Thickness and SNR**
Increasing the slice thickness will increase the SNR. Increasing the slice thickness increases the voxel size which results in an increase in the amount of signal received by the individual voxels. But this would however reduce the spatial resolution.

**Matrix Size and SNR**
Increasing the matrix size will reduce the SNR. Increasing the matrix would reduce the voxel size, reducing the amount of signal received by the individual pixels. Smaller pixels will receive less signal and produce a low SNR image. Correct selection of matrix size for a particular FOV is necessary for optimum quality images.

**FOV and SNR**
Increasing the FOV will increase the SNR. It would increase the pixel size which will increase the number of signals received by individual pixels. Large pixels would receive more signal and produce higher SNR images. Increasing FOV would however reduce the spatial resolution and produce blurry images. To achieve max spatial resolution, the matrix size must be increased when increasing the FOV.

**Number of Averages and SNR**
Number of averages is used to represent the number of times data is repeatedly acquired to form the same image. Increasing the averages will increase the SNR. Doubling the averages will increase the SNR by square root of 2 and double the scan time.

**NSA and Slice Thickness**
Decreasing the slice thickness in high resolution images will reduce the SNR. Increasing the NSA would increase the SNR. When reducing the slice thickness, the signal will drop. So, to compensate for this drop, the NSA needs to be increased but this would in turn increase the scan time. But this would be the most appropriate method when reducing the slice thickness without compromising the image quality.

**NSA and FOV**
Decreasing the FOV will reduce the pixel size and produce an image with low SNR. To compensate for this signal loss, either the matrix size needs to be reduced or the NSA must be increased. Decreasing the matrix size will slightly reduce the image quality while increasing the NSA would improve the image quality. The only downside is the significant increase of the scan time.

**NSA and Resolution**
Increasing the matrix size will reduce the pixel size and produce a low SNR image. To compensate for the signal loss, the NSA can be increased. Increasing the matrix size and NSA would increase the scan time. Increasing both parameters would nearly triple the scan time, but the result will be a very sharp and detailed image.

Different settings can be adjusted to manipulate a grainy/blurred image as shown in Table 2.1 and Table 2.2.

| **Grainy Image** |
| --- |
| - Reduce the base resolution. This would reduce the scan time<br>- Increase slice thickness. This will increase the voxel size and SNR and thus the image will become smoother<br>- Increase number of averages. This will increase the scan time though<br>- Increase FOV. This will increase the pixel size and SNR and thus the image will become smoother |

**Table 2.1:** Settings adjustments for grainy image

| **Blurred Image** |
| --- |
| - Increase resolution. This would increase the scan time.<br>- Decrease FOV. This would reduce the pixel size and SNR and the image will thus become sharper. |

**Table 2.2:** Settings adjustments for blurred image

# 3

# Paper Materials and Moisture Transport

## 3.1 Paper materials

Paper materials are produced from wood which has been turned into a fibrous pulp through one of various either mechanical or chemical pulping methods; the pulp is further processed to selectively modify the end product material properties and dried into paper sheets. Mechanical pulping separates cellulose fibres from wood physically while chemical processes, such as the commonly used 'kraft process', use a mixture of chemicals to achieve this separation [3]. The pulp consists of individual fibers, each being a long and slender structure typically in the range of 10-50µm wide and 700-4000µm long [18].
The centre of the fibre is hollow, with the fibre wall having a structure as visualised in Figure 3.1. The fibre is composed primarily from components cellulose, hemicellulose and lignin [3].

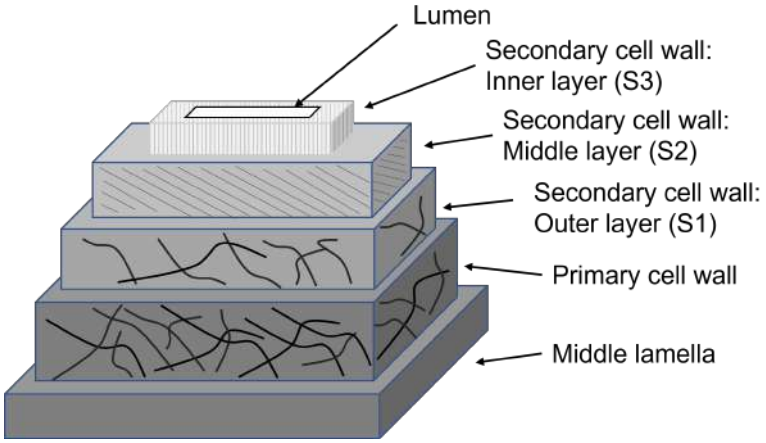


**Figure 3.1:** Hierarchical structure of a paper fibre visualising from the fibre's outer layers to inner lumen

The fibres mechanical and chemical properties depend on various factors such as wood species, wood growth section and processing which all can alter relative fractions of the three primary components. Common pulp processing steps in addition to initial pulping include bleaching to remove lignin and achieve brighter and

whiter pulps. The addition of chemical agents change paper absorption characteristics, filler additives can be added into the paper pulp or different pulp types mixed to attain specific pulp properties.

As pulp is dried and rolled, higher density networks of fibres and bonds are formed. The density of the network, distribution of pulp fibre types, sizes or chemical properties and the thickness of the material layer can all be optimised for the desired paper application. Paper production commercially leads to a preferential fibre orientation along the direction of motion leading to orthotropic paper products. Moisture transport and mechanical properties are thus direction dependent. The 'machine direction' (MD), 'cross direction' (CD) refer to the running direction of the paper through machines during production and the direction perpendicular to that through the same plane while the through-thickness direction (ZD) refers to the thinnest dimension of the paper. This can be visualised through Figure 3.2.
Coatings can be added to the paper material during production to achieve improved

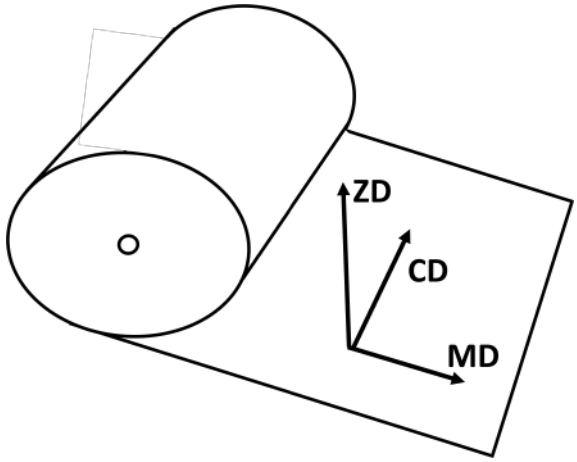


**Figure 3.2:** Machine, cross and through-thickness direction within paper production

glossiness or improved print-ability on the paper surface as is common for packaging applications. Furthermore, paper grades can be layered to achieve a desired material design.

## 3.2 Moisture-paper material interaction

Paper at the basic level is a heterogeneous fibre mesh with a certain surface roughness and porosity [24]. As a natural cellulosic material, paper has a strong tendency for water absorption due to cellulose fiber's intrinsic hygroscopic nature [26]. The material structural and chemical characteristics, liquid properties as well as their respective interactions determine liquid transport through fibrous materials. In this investigation, water imbibition at ambient temperatures will be explored without analysis of temperature effects.

Paper material has commonly three proposed liquid populations; these being water vapour, interfibre (pore) liquid as well as liquid sorbed within fibre structure itself that interacts to a greater extent with the fibre polymers[1] [2] [9]. Dynamic exchange and transport between these populations is naturally occurring as non-equilibrium mass exchanges. These liquid populations can be visualised in Figure 3.3 which displays the relative positions of these water populations within a simple fibre structure of paper.

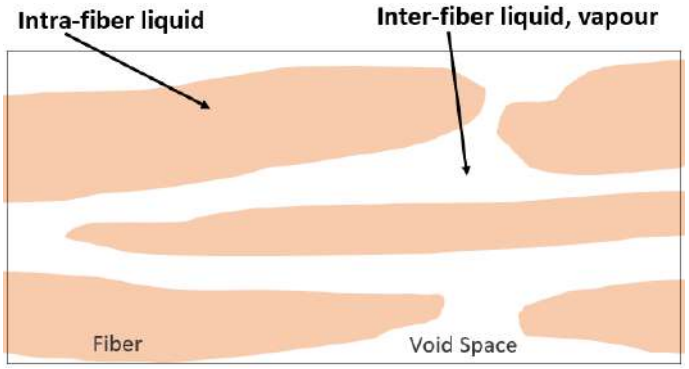


**Figure 3.3:** Liquid populations within paper fibre structure

The size of the interfibre space is highly variable due to a wide range of production variabilities as well as material design factors within the stochastic fibre media. Interfibre pore space is able to impact both capillary liquid as well as vapour uptake. A second independent pore space stems from pores within the fibre wall itself. This pore space is, due to removal of lignin and hemicelluloses during pulping, higher for pulped than unpulped fibres which allows for a high liquid uptake before saturation for processed fibres [1]. When fibres are water saturated, water is a significant component of the cell wall typically greater than 1 gram water per gram dry fibre [24].

In packaging and paper straw applications there is the potential for high moisture contact with the paper material. For packaging materials, this contact is, due to polymer layers often being in contact with the contents rather than the liquid, most significantly during the packaging material liquid sterilization step for aseptic packaging. For paper straws this contact is through direct liquid contact with the straw during usage. High material liquid contents however lead to undesired mechanical strength degradation which can be a hurdle to packaging performance and cellulose fibre application or durability [24] [5]. This degradation stems from both the loss of fibre network structure through fibre cohesion loss as well as loss of individual fibre strength and stiffness [2]. For this reason pre-treatment of fibres can be conducted during paperboard production for increased material hydrophobicity known as 'sizing.'

Sizing of materials is a treatment with hydrophobic materials such as rosin, alkenyl succinc anhydrine (ASA) or alkylketene dimer (AKD), which reduce the wettability of fibers [26]. These additives modify the fibre surfaces to attain a larger water contact angle. Sizing can be optimised towards the desired hydrophobicity or

wetting resistance of the end use of the paper product with (Xu et al., 2018) indicating in [26] that sizing is typically particularly effective at reducing perpendicular penetration into the paper surface. The article [24] can be referenced for a thorough outline of available hydrophobization methods.

Two types of water invasion of paper materials are the in-plane invasion of water into the thin porous material with vertical liquid uptake known as 'edge-wicking;' as well as water invasion in the through-thickness direction from a single paper material face. These two different moisture movement pathways are visualised through Figure 3.4. Both uptake types will form part of this work, with a more significant focus being on through-plane direction liquid uptake.

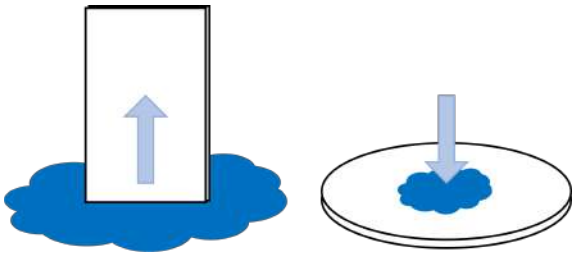

**Figure 3.4:** In-plane liquid uptake as compared to through-plane water invasion

Moisture can enter the fibre structure as a liquid or a vapour, it can interact with the fibre surface or enter the fibre structure itself. Liquid imbibition rates depend on factors such as pore size, porosity, permeability, tortuosity, evaporation and liquid contact angle [25]. Furthermore, properties of paper such as its dimensional stability, surface roughness and strength change with liquid content [24].

Work by (Salminen, 2008) in [23] found that the pore transport rate is more impacted by the expanded fibre matrix-rather than the dry fibre matrix. The moisture transport through materials is in this way a strong function of the material moisture content. The mechanisms through which this moisture uptake occurs are discussed in 3.2.1 - with individual proposed mechanisms highlighted.

### 3.2.1 Moisture transport mechanisms

Moisture transport through the porous cellulosic fibre layers has been described as occurring through two pathways simultaneously- the diffusion of moisture and vapour through interfibre void spaces and intrafibre diffusion of sorbed moisture through the cellulosic fibres themselves [5]. These apply to both in-plane and through-plane liquid transport, with the majority of currently published research focusing primarily on the in-plane transport.

There is debate in literature what these exact mechanisms for water transport within paper materials are, however a concise summary can be that of [16] [23] [24]:

1. Diffusion of vapour though paper pores

2. Capillary transport of liquid in the paper pores
3. Diffusion of sorbed moisture through the fibres

These transport mechanisms have been described mathematically; however their respective weightings are not conclusively defined for any of the large range of paper materials largely due to the lack of spatial moisture distribution data within paper samples during moisture uptake [14]. More definitive measurements of this intra-sample distribution, as is hypothesized can be obtained through an MRI, will thus be significant.

The importance of the different mechanisms are seen to be functions of temperature, moisture vapour pressure and composition as well as the chemical and structural properties of the fibres [9][16][24]. Moisture transport can thus for a certain set of conditions be modelled as a combination of these mechanisms with one commonly being rate determining.

It is debated in literature which mechanisms are dominant through differing paper types. For two distinctly different paper categories, namely sized and unsized papers, a common conclusion drawn is that pore diffusion (mechanism 1) and capillary transport (mechanism 2) are dominant for unsized paper while pore diffusion (mechanism 1) is dominant for sized paper grades (more hydrophobic) [26][3] [20, pg. 196]. The work of [26] as well as [20, pg. 195] and contained sources corroborate this, additionally indicating the importance of diffusion within the fibre wall itself (mechanism 3) to this moisture transport, notably for sized paper grades.

The difference between hydrophobic and hydrophilic paper materials has to do with the surface energy and resultant contact angle that the moisture makes with the material fibre surfaces within the pores. The well known capillary effect leads to a natural uptake of moisture at contact angles lower than 90°while a significant uptake reduction or even liquid discharge at contact angles greater than 90°. This concept is explored further in 3.2.1 with a visualisation of the contact angle found in Figure 3.5.

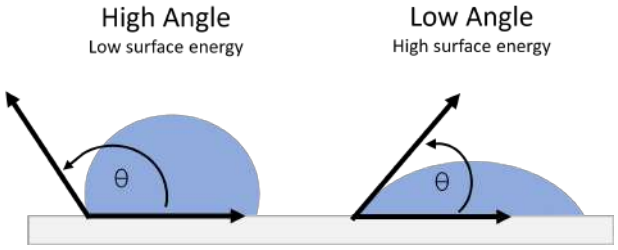


**Figure 3.5:** Contact angle visualisation

Results indicate that in-plane moisture transport within highly sized paper grades was influenced by factors other than the size level [26]. This emphasizes the importance fibre structure has on moisture transport in the sized case. This

fibre structure could be a function of the fibre density, the fibre wall thickness and the fraction of collapsed lumens, the fibre flexibility and inter-fibre bonding. A higher density for materials such as the sized materials tested in this work mean a higher density of fibres. This could be an asset to improving moisture transport as contact between fibres aids the interfibre transport of intrafibre fluid that as such does not need to pass through interfibre pores. Fibres with thinner walls can also be more prone to collapsed lumens, leading to closed lumen transport channels. [26].

### Diffusion of vapour though paper pores

Vapour diffusion occurs through the movement of liquid vapour through pore pathways in the fibre structure due primarily to moisture concentration gradients. A major influence on this vapour transport stems from material permeability. As permeability of a material increases this allows for more effective vapour transport.

Permeability on a macroscopic level is influenced notably by the effect of porosity amongst other effects for fibrous materials, most notably as porosity approached zero [3]. Permeability, due to the anisotropic nature of fibrous paper, is an anisotropic property having higher permeability in the paper's machine direction than cross direction. Work of (Leisen, 2002) [14] has indirectly inferred the extent of this mechanism to be the faster mechanism for transport through sized paper in a humid atmosphere based on MRI imaging with moisture within the pores subsequently able to be adsorbed by the fibre. Thus the actual measurement was on absorbed liquid moisture as opposed to the vapour itself.

### Liquid capillary transport

Liquid capillary penetration into the porous fibre structure is most important for transport in unsized paper and is a strong function of material permeability. The capillary pressure is generated on capillary walls of the paper stemming from the mutual attraction of molecules from the liquid (cohesion) and molecules of the solid (adhesion)[24]. A positive capillary pressure leading to water entering the fiber matrix stems from a liquid phase-solid phase contact angle of less than 90°. Conversely, a negative hydrophobic contact angle is lower than 90°as visualised in Figure 3.5.

Hydrophilic pores imbibe liquid progressively from the smallest pores which have the larger attraction forces to the largest pores. Conversely the hydrophobic pores take up water starting from the largest pores due to larger repulsive forces within the smaller pores provided the external load is sufficient to overcome repulsive forces [2]. The actual measurement of contact angle of sample materials is only able to be measured on the liquid surface and thus this is a surface contact angle and not an internal fibre matrix contact angle. This is however taken as a measure of the entire matrix's surface properties. The sample materials tested in in this work are all hydrophobic with contact angles greater than 90°.

#### Diffusion through fibres

Movement of fluid within the fibres referred to commonly as fibre diffusion occurs in a manner not entirely understood through literature, however describes moisture movement of liquid closely interacting with the fibre and fibre cell walls themselves [2]. Isolating this mechanism from the other mechanisms is not trivial and thus leads to the lack of understanding of this tortuous network flow. This movement is naturally assumed to stem from gradients either chemical or moisture based [2].

This mechanism has notably been found to be significant when analysing sized paper fluid transport [20, pg. 206]. The rate of moisture transport within the fibre once liquid has been taken up is likely of a similar magnitude between sized and unsized paper grades. This is as sizing impacts only external fibre surfaces.

### 3.2.2 Moisture uptake effects

During flow of aqueous liquids through fibre networks, expansion of the network is experienced in part due to hydroxyl groups (-OH) in the fibre combining with water molecules [8]. Due to this and the breaking of intra-fibre hydrogen bonds upon water molecules' entrance into the fibre walls and between hydrogen bonded fibrils; the pore structure of the fibrous material changes. The saturation limit of water uptake and imbibition dynamics change along with this pore structure change [24] [23] [1]. As the amount of water taken up increases, the internal bonding of the fibre wall decreases. This internal bonding of the fibre wall decrease allows an increase in the distance between cellulose chains and thus causes swelling[24]. Fibre network expansion influences water transport in two major ways- its effect on the transport velocity of the liquid front and the thickness of the penetrating water front relative to the dry sample [23].

It can be suggested that the thickness of swelling in paper can be used to estimate fibre sorption [23, pg. 21]. An increase in inter-fibre distance is responsible for the swelling of wet paper according to [8], which means that the increase in volume of inter-fibre pores determines paper volume expansion. This increase in volume must stem from water uptake, and thus the quantity of water is relatable to the volume change.

# 4

# MRI Application within Paper Materials

MRI has been an experimental technique employed on thin films and paper materials through a selection of applications such as moisture uptake in a humid atmosphere, material drying, liquid quantity and diffusion assessment. The value of the technique comes in its non-invasive, non-destructive, and quantitative nature which makes it possible to measure processes while things are changing with time and not only the result of the process [17]. This instrument however has significant untapped potential.

## 4.1 Moisture transport focus using MRI

### 4.1.1 Drying

First works into MRI application were gained assessing moisture gradients within cellulose fibre networks. Nilsson et al. assessed the water distribution within a cellulose pulp sheet dried in-situ. Here a spatial resolution of 390$\mu$m was attained through the 4mm thick sheet [17].

Work done by Nilsson et al. showed that magnetic resonance imaging was suitable to study drying in thin films [17]. In their work, sodium silicate films were studied and was found to attain both molecular mobility of water as well as density information with a high spatial resolution. It was observed that a moisture gradient formed across the sample through the progression of drying, which was not fully understood then. The distribution of moisture in industrial pulp samples during drying was studied by Bernada et al [6]. Copper sulphate was used as a contrasting agent to reduce the T1 relaxation time which made it possible to detect moisture at low water contents (6%). A spatial resolution of 150$\mu$m was obtained in the through thickness direction of the sample [6]. This is almost a 2.5 times increase in comparison to what was achieved by Nilsson et al. However, at the same time the acquisition time increased by around 4 times [7].

Drying in cellulose based materials specifically was studied by [11] to measure quantitative water profiles during drying of liquid packaging board. Relative liquid concentration measurements were made through 1D imaging with a spatial resolution of 15$\mu$m per pixel in a 2mm field of view; 6 averages were taken per image

leading to a 24s imaging time. Due to the importance of imaging procedure in attaining representative measurements, this was a focus of Harding's work [11]. A similarity to the current work is that fast acquisition is attained using 1D spin-echo measurements. Water within cellulose fibres has a very short T2 relaxation time typically between 1 and 6ms with lower water contents leading to lower relation times. The echo time within the spin-echo sequence however must be smaller than 5 times this T2 relaxation time to avoid signal attenuation. For any 1D measurements, notably through thin materials, the field of view must also be perpendicular to the sample to avoid result distortions [11][19].

Leisen et al. conducted similar work assessing the degree of anisotropy in paper's in-plane diffusion [13]. Previously, not much work had been done to study the in-plane diffusion of moisture in paper. A notable finding here was of the difficulty in attaining signal from paper with a moisture content under 6%. Both the work of Harding and Leisen (2001) started with soaked samples and thus positioning was not an issue. In this current work the sample is initially dry and thus positioning needs to be guaranteed without the use of a reference image before testing. Both also had comparatively thick samples simplifying the measurement.

### 4.1.2 Moisture uptake

Leisen et al. did start with dry samples assessing rather moisture uptake from a humid atmosphere in the through-plane direction and was able to find support to the idea of moisture transport of paper being through two steps, the water vapour ingress into pores and subsequent sorption into fibres [14]. A TE of 1.4ms and TR of 2s for 2D images were used for 2mm thick samples, however due to low signal-to-noise ratios 68 mins were required for imaging of single face moisture uptake while 17 minutes for dual face moisture uptake. In the current work the samples are to be at maximum 0.4mm thick and multiple images are required per minute to attain functional data, most notably within the initial period of moisture uptake. Some notable findings of Leisen et al. were that for the paper samples investigated, the water was found to diffuse faster in vapor and the sorption of moisture by the fibers was at a slower rate [14]. A good takeaway from this work was that intrafiber diffusion of moisture is quite important during the transport through paper over longer duration.

Perrin et al. improved on the work of [14] for uptake of paper looking into uptake of ink deposited on paper [19]. In Perrin's work a spatial resolution of 10$\mu$m and temporal resolution of 1.3 seconds per image was attained on a sheet 100$\mu$m thick. Furthermore, [19] showed that the buckling of paper due to moisture could show irregularities in the 1D profiles.

A further difference of this current work when contrasted to previously conducted work such as [19] as well as [11][13][14] and similar papers is the requirement not to maximise the signal quantity attained, with the signal attained being due to the reference sample, but rather identifying and isolating the signal stemming from the sample as contrasted to the signal stemming from the surrounding liquid.

This poses the challenge not to be one of selecting correct MRI imaging settings or sequences but rather developing a methodology with which such measurements can be reliably taken and result outcomes can be processed effectively.

### 4.1.3 Diffusional transport

Samyn et al. indicates the importance of diffusional transport for hydrophobic papers [24, pg. 6459]. Diffusion through paper was measured both in the plane and through thickness directions by NMR pulsed field gradients. Diffusion coefficients were not found to be impacted by fibre dimensions, internal fibre structure or chemical composition but were found to be consistently higher for the in-plane rather than through-plane directions. A slow and a fast diffusion coefficient distinction were found.

Perkins et al. similarly makes use of NMR techniques to investigate diffusional transport with paper fibre structures [18]. This work was built on two sets of work. The first by Li et. al. in [15] who distinguished between two diffusional regimes in paper with high moisture contents (>4g/g) that of bulk water and interacting water. The diffusion coefficients were found to be $1.3 \times 10^{-9} m^2 s^{-1}$ and $4 \times 10^{-10} m^2 s^{-1}$. The second work was done on low moisture (<0.25g/g) content cellulose fibres (ref topgaard and Soderman 2001 from in Perkins) who rather found a single phase of water with significant water-cellulose cross-relaxation obtaining typical diffusion coefficients from $10^{-10} m^2 s^{-1}$ to $10^{-11} m^2 s^{-1}$.

Perkins et al. examines intermediate moisture contents between 1.2g/g and 0.2g/g and found that as the moisture layer on fibres thickens with increased moisture content, liquid layers are distanced from fibre interaction and thus can exhibit more free diffusional mobility [18]. It was found that diffusion coefficients decrease linearly with decreasing moisture content similarly to the findings of Harding et al.[11]. It is also found that through-plane diffusion has an increase in liquid-fibre interaction effects and tortuosity with diffusional motion when compared to in-plane diffusion.

# 5
# Methods

## 5.1 Equipment

All experiments were performed using a Bruker Advance-III HD NMR spectrometer having a magnetic field of 7T with MiniSWB90 single-tuned $^{1}$H quadrature probe with 66mm in diameter. Standard spin echo sequences were employed. The data was collected using Paravision 6.0 software by Bruker and was then imported into Matlab for data processing and analysis.

**Figure 5.1:** MRI instrument

## 5.2 Materials

The materials tested in this work are paperboards made use of industrially during the production of packaging cartons. A summary of the materials tested is available

in Table 5.1 with descriptions of the materials to follow.

| Material Descriptor | Outline | Sizing | Thickness ($\mu$m) |
|---|---|---|---|
| B | Duplex uncoated (bleached+unbleached) | sized | 360 |
| B2 | Duplex coated (CLC) (bleached+unbleached) | sized | 360 |

**Table 5.1:** Summary of materials assessed

Initial tests and proof of concept tests were conducted on an unsized 'egg carton' like material which had a high water uptake. This material was some compressed pulp that was not made in a paper-machine. These tests were mainly done to be able to develop the test method and contrast with thinner and sized materials. Making use of the egg carton material initially allowed development of the experimental method with regards to MRI settings and positioning problems within the MRI before further testing on applicable samples. The egg carton material had a very inhomogenous and hydrophilic surface with multiple material layers stacked on top of each other. This allowed for a fast water uptake and even led to air pockets within the surface. Figure 5.2 visualises the structure of the material surface.

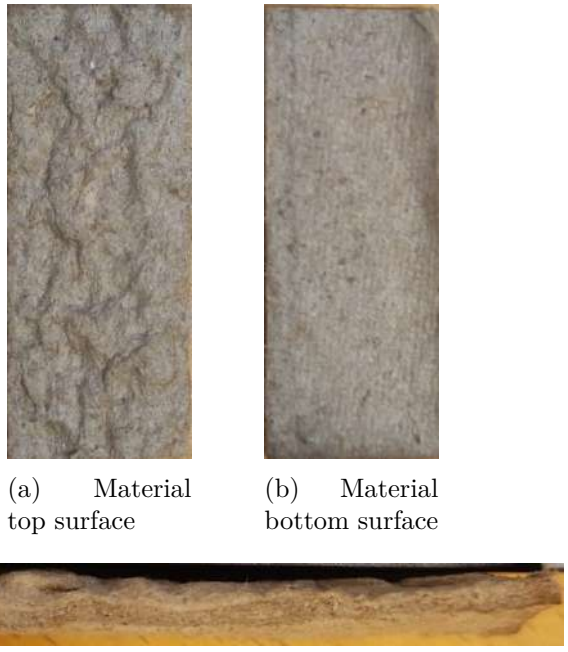

(a) Material top surface

(b) Material bottom surface

(c) Through-thickness

**Figure 5.2:** Egg Carton Material

There are two independent packaging materials considered through this testing. These are considered based on the experimental consideration of their differing

hydrophobicities as well as surface properties. These materials are listed in Table 5.1.

The duplex materials consist of a combined dual layering of top bleached and bottom unbleached pulps forming a single material composite. This dual layer is visible to the naked eye as per Figure 5.3; both origin pulps however attain same sizing during production.

**Figure 5.3:** Visualisation of sample paperboard's top and bottom faces due to its double layered construction (Material B pictured here)

The fibre structure of the materials can be seen through SEM images of the material surfaces. The images, taken on a Phenom ProX tabletop SEM, provide a tangible representation of the fibre structure that is being considered and can be used as a strong basis to understand the mechanisms at play during moisture transport. Figure 5.4 shows a representative element of the material B's sample surfaces.

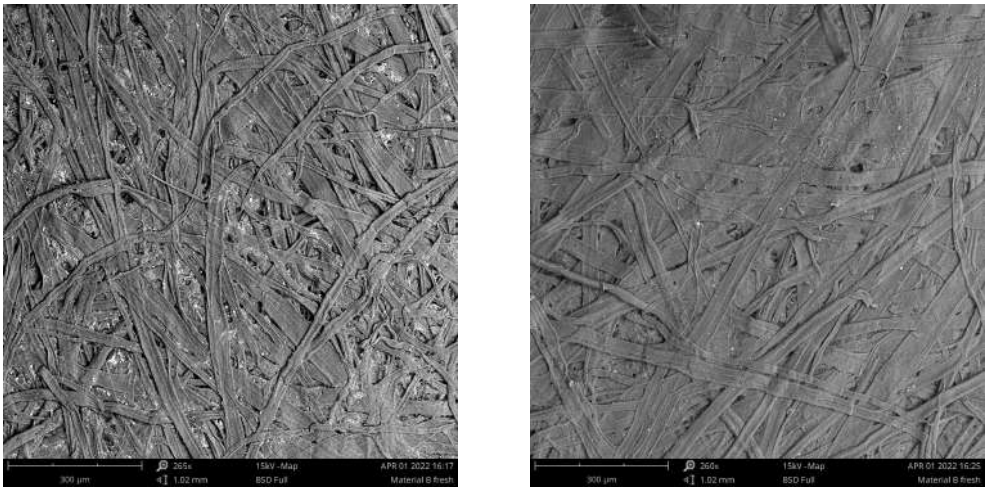

(a) Bleached pulp surface (b) Unbleached pulp

**Figure 5.4:** SEM images of top surface of Material B

Figure 5.4 shows how compact the fibre structure is and how compression during production has influenced the fibres. The distribution of fibre sizes is evident in Figure 5.4 with a significant distributional range by design however this property of the material is unknown through this work due to supplier reserved information. Additives to the fibre structure are further visible in the figure in the form of the brightly responding white granules visible. These are mineral fillers that are added by the suppliers during the paper making process.

Material sample B was an uncoated material, while in contrast material B2 has one of its faces coated with a clay layer. This layer aids surface printability and is visible in Figure 5.5.

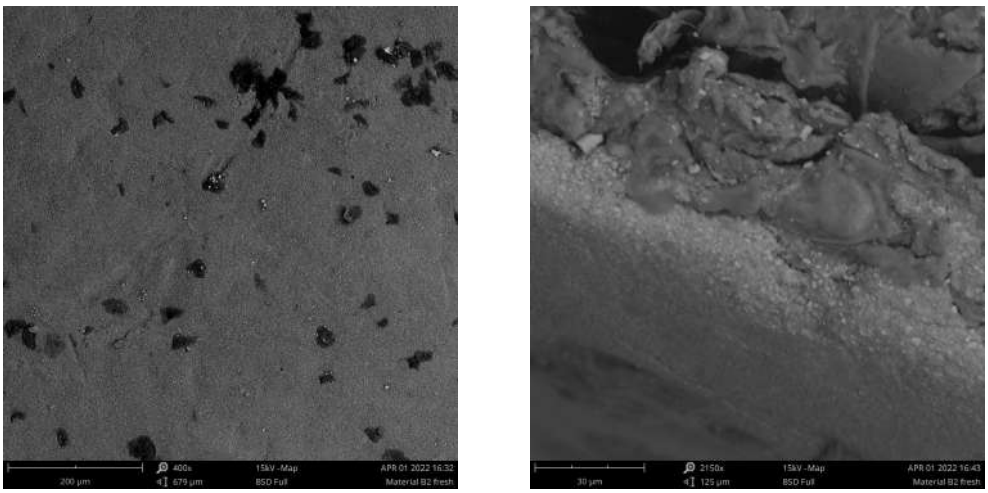

(a) Bleached pulp surface with clay coating

(b) Through thickness image

**Figure 5.5:** SEM images Material B2

The clay layer is evident in Figure 5.5 in how it smooths the finish of the paper in contrast to what was seen for the uncoated material B. This clay based layer is porous by nature and thus moisture absorbent. It is of interest in this work to assess the impact this absorbent material surface has on the moisture transport dynamics not only with reference to through thickness but also edge-wicking applications.

## 5.3 Testing procedures

The scope of this work is an exploration of the potential that the experimental technique MRI has for non-invasive measurement of moisture transport through porous paper materials. Method development presented here for this reason forms a large part of the functional knowledge progression and outcome of conducted work. The testing procedures below present the practical application of these methods.

### 5.3.1 Visual edge-wicking

Edge-wicking is the in plane liquid penetration into a paper sheet. Many efforts have been made to reduce the effects of edge-wicking over the past few years [26]. Most of the solutions mainly involved chemically modifying the fiber surface and increasing the sizing of the material. Higher sizing allows for reduced capillary penetration of water through the sample [26]. However, it is not possible to increase the sizing over certain levels due to food safety concerns and cost.

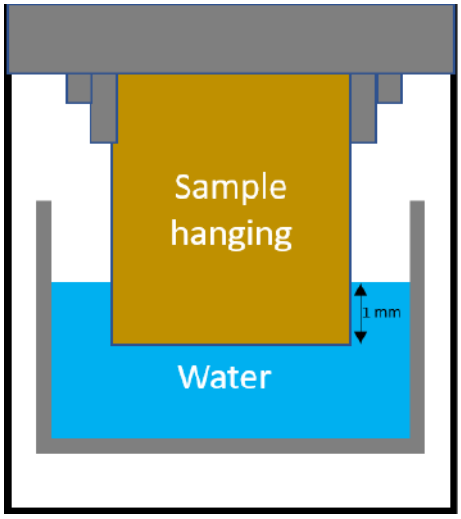


**Figure 5.6:** Graphical edge-wicking diagram visualising the experimental setup of an edge-wicking experiment

Visual edge wicking tests were first conducted using a camera. This was done in order to make appropriate choices for the settings in the MRI. The camera was set up to take a photo every 1 minute under artificial lighting. The sample was dipped in water up to 2 mm height to allow for the edge-wicking. Coloured water was used to provide a visual indication of the waterfront. These tests were done for both a sample in open air and confined conditions to prevent surface evaporation. The coloured water does contain additive and could lead to minor impacts on the wicking characteristics, however these are considered negligible for the purpose of these tests.

### 5.3.2 MRI in-plane measurements

Observing edge-wicking of different samples within the MRI would potentially provide useful information on the material characteristics and properties. The method of testing was developed for the MRI based of the visual tests and tested on the egg carton and Material B. The development of the methodology is outlined below.

#### Method Development

3-D printed rigs were used in the MRI which were provided by Tetra Pak®. The rig involved 3 individual pieces which included the sample holder (which supported

the sample to be wicked), the main body which would allow for consistent sample holder insertion and positioning relative to the cup holding water. This cup would be twisted into the main body so as to come into contact with the sample holder placed at the top at a defined manually initiated time. This experimental setup is as per the diagram in Figure 5.7.

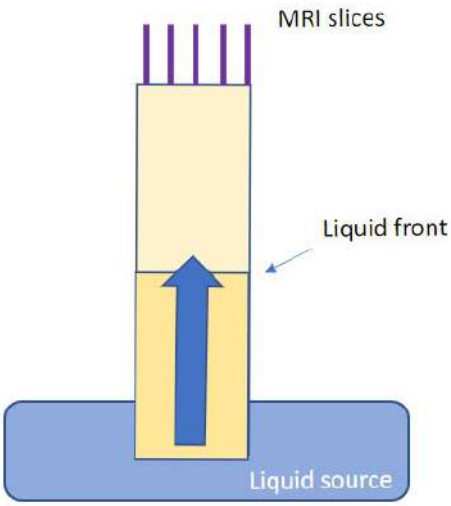


**Figure 5.7:** Graphical diagram visualising the experimental setup of the MRI edge-wicking experimental rig

This experimental set up is made up of the components as per Figure 5.8. The development and modifications of the rig can be seen in Appendix A.

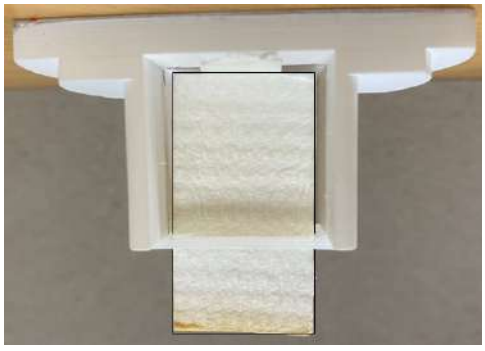

(a) Sample holder

(b) Main body

(c) Water cup

**Figure 5.8:** Edge wicking rig parts used in the MRI

This initial setup was effective but could not be used as the final design due to positioning errors and stability issues arising when moving the cup containing water in place every test. Furthermore, the removal of the entire probe from the MRI after every test made it difficult to get consistent results.

In order to minimize these errors, modifications were made. A new sample holder that had longer arms which improved the sample stability during testing reducing the potential for the sample angling a certain direction during testing (a comparison is found in Figure A.4). Furthermore, a simple setup was constructed using cardboard layered rolls which allowed the main body of the rig to be held in place within the MRI and to be controlled from the outside by an operator. This was done in order to avoid removal of the MRI probe each time, instead, only the tower of the cardboard rolls would have to be removed from the rig in between each test. These modifications allowed for the cup holding the water to slide in through the tube of cardboard rolls, into the main body of the rig to have the sample dipped at the top as seen in Figure 5.9.

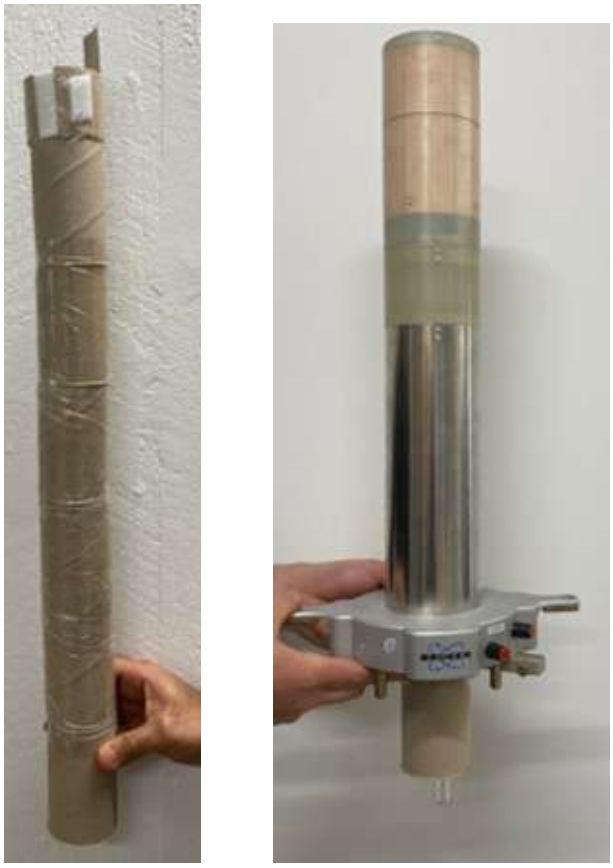

(a) Cardboard roll tube

(b) Setup in MRI probe

**Figure 5.9:** External control of rig

### 5.3.3 MRI through-thickness measurements

A Cobb test is a well known experiment conducted over a time-frame of commonly 60 or 180 seconds during which time liquid penetrates a material sample from a single face. The Cobb test is in this way a standardised testing procedure that focuses on the through-thickness transport of moisture within the sample. It is

useful in determining the amount of water absorbed into the surface of a sized paper sample/paperboard in a set period, usually 60/180 seconds. This type of tests are used in papermaking since it quantifies the ability of the paper sample to resist the penetration of moisture into the paper from the surface.

### Method Development

Since the measurements are taken with the help of the MRI, the typical setup for a Cobb test was not able to be followed exactly due to the presence of metallic materials in it, and also the size of the standardized test does not fit in the equipment. As was the case during edge-wicking testing, an initial iteration of an experimental testing rig compatible with the MRI apparatus was thus 3D printed from which base development work was conducted. Due to the high spatial resolution desired when measuring water transport in through-thickness direction, development of the experimental set-up and methodological design was a significant portion of the overall thesis work. A summarised elaboration on this development is found in Appendix A.

Figure 5.10 presents the experimental setup found most effective for accurate Cobb style moisture measurements within the MRI. The final developed rig consists of 4 main parts that are connected/stacked and then inserted into the probe in the MRI. The individual units of the rig can be seen in the figure 5.10 (a) as the blue material supporting base; a rubber seal with a 1cm x 1cm square cutout, a white 3D printed platform with the same cutout and the top connector/support that is fitted with a sealing rubber O-ring.

The square cutouts are primarily to reduce the sample surface area exposed to the water during testing and allow for a square liquid contact area. This was implemented primarily to reduce the effects of buckling of the paper sample and to also reduce the field of view in the MRI to eliminate unwanted signal as well as having the slices of the MRI align only with the required area of interest. The rubber seal helps in keeping the water contained within the 1cm x 1cm block and thus prevents the water from escaping through to the sample's edges and seeping into the sample outside of the selected liquid contact area. The 3D platform keeps the rubber seal in place and helps in applying pressure on the rubber seal when screwing the top in. This again helps with keeping the water contained. Lastly the top is equipped with an O-ring to pressure on the entire stack of parts when screwed in and stop water from escaping down the sides if it were to overflow from the 1cm x 1cm block.

About 2ml of water was injected into the rig from the top. Initially, the water was injected and then the rig was placed into the MRI and only then the measurement was started. In doing so though, quite a bit of time was unaccounted for before the first measurement taken by the MRI, especially when the temporal resolution was around 2 min. To solve this issue, water was injected the second the measurement was started in the MRI. This was done through a syringe connected to a long PVC tube which was first attached on top of the rig, inserted into the MRI and then have water injected just after the measurement was started. This setup can be seen in 5.11.

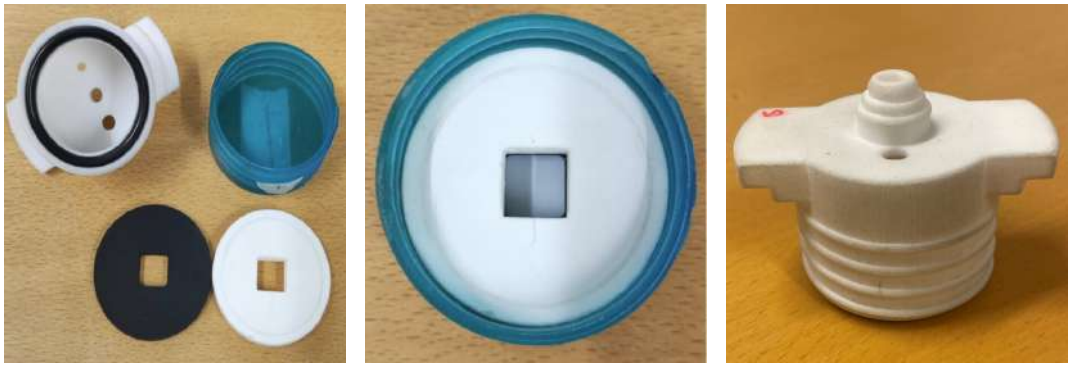

(a) Individual rig units (b) Stacked sealing setup (c) Top support for connection with the sample base

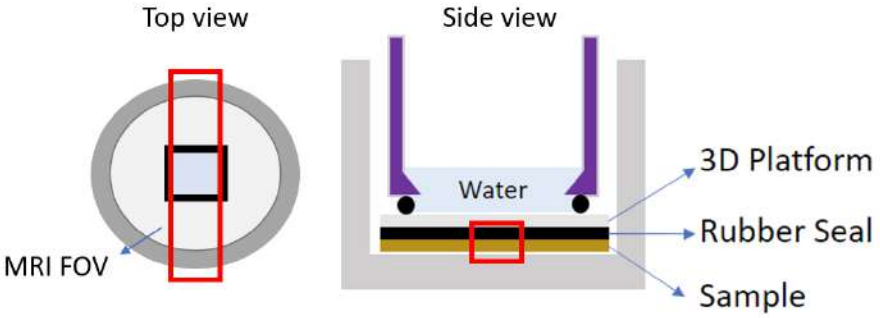


(d) Conceptual rig design

**Figure 5.10:** MRI Cobb Testing Setup for MRI

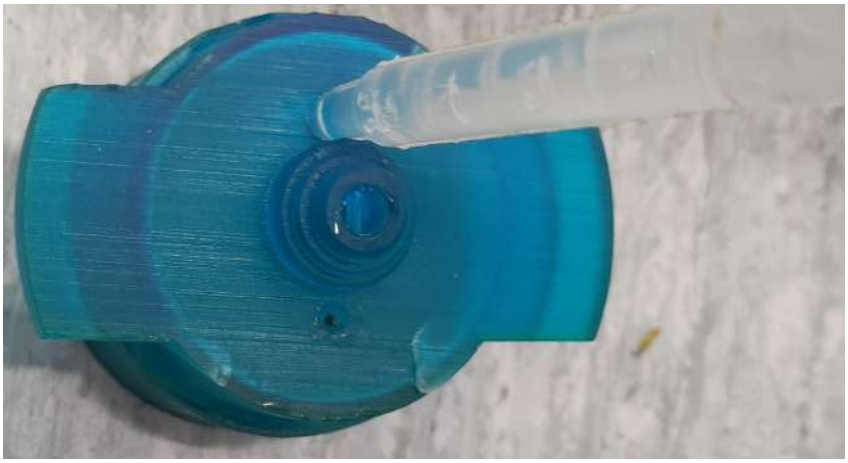

**Figure 5.11:** Water injection setup

Multiple tests were conducted with hydrophilic egg-carton material for method development before conducting testing upon paperboard sample material. Multiple sample acquisition times and testing optimisations were conducted and the 1D profiles of these were constructed and analysed using Matlab.

**Optimisation of MRI parameters:**

Various comparison tests were performed in order to optimise the Signal-To-Noise Ratio (SNR) for the Multiple Slice Multiple Echo (MSME) 1D profiles. As mentioned in Chapter 2, the different settings in the MRI are interconnected and affect the signal received. The echo time (TE) was constantly kept at the lowest possible time in order to reduce the effect of T1 as much as possible. The image size was also set to 128 points as at higher resolutions (of for example 256 points), the signal to noise ratio is too low. This is due to the fact that the paper samples being tested take up very little moisture which provides the MRI receiver a much lower signal at the higher resolution for the same temporal resolution. Using the higher image size would require increasing the number of averages to get a better signal hereby increasing the scan time significantly which is not preferred in this situation. Multiple experiments were carried out at various repetition times (TR), FOV, slice thicknesses and averages. Since each setting affects the signal to noise ratio, priority had to be given to the settings that should not be changed and then the other settings were optimised around it. In this case, the TE and image size was fixed as discussed before, and all the other settings were optimized around it. A summarised view of this testing's outcomes are found in Appendix B.

Firstly, the TR was optimised based on the T1 of water which is around 2-3 seconds. Thus, the TR had to be at least 2s long. Keeping this in mind, various tests were run at different TRs from 2s to 5s. These results concluded finalisation the optimum TR to be 2s long. Based on the image size being 128 points, the FOV was optimised around it. Ideally having a lower field of view allows for more number of points within the actual thickness of the sample which is advantageous. But at the same time, a lower field of view meant lower SNR which is not preferred. Considering all these effects it was decided on having a field of view of 4mm which gave a spatial resolution of 31.25 $\mu$m per point and approximately 11 points through the thickness of the sample. The other potential field of views considered and their respective spatial resolutions can be found in Appendix B.

# 6
# Results

## 6.1 In-plane moisture transport

Edge-wicking styled in-plane liquid uptake by paper materials is a commonly used measure primarily for characterisation of unsized paper materials. This current work focuses on sized materials for application within the packaging and straw industries, and it is investigated whether in-plane analysis can provide new insight into sized material liquid uptake. Edge-wicking as a process is generally seen to occur to a far lesser extent within more hydrophobic materials due to the importance of the capillary liquid uptake mechanism in edge-wicking as discussed in 3.2.1. Analysis both through visual testing and MRI measurements of in-plane liquid uptake is conducted, outlining the potential MRI has to expand understanding of in-plane liquid uptake for paper materials.

### 6.1.1 Unsized material in an open atmosphere

Initial testing for methodology validation was conducted on unhydrophobized materials such as egg-carton material. This material has a comparatively high rate and extent of moisture uptake when compared to the focus materials of this work with the liquid uptake fronts of the material being clearly visible to the naked eye during edge-wicking tests. The use of hydrophilic materials can for this reason be used as a baseline for method development. This could then be used to validate the possibility of measurement of the sample materials within an MRI context. Figure 6.1 visualises how MRI is an applicable tool for measurement of such liquid uptake. The figure represents successive MRI liquid water measurements within the rectangluar sample volume over a short 2 minute period in the experimental setup orientation as per Figure 5.6.

In the figure it can be seen that within the hydrophilic egg carton material there is a fast progressive uptake of liquid in the form of a liquid gradient inferred from the signal intensity. The first 12 second measurement displays a steep drop-off in signal intensity, which is representative of liquid uptake, extending from the position 0mm liquid interface to the sample reaching a negligible liquid content just under 2mm above the liquid surface. This drop-off represents a combination of the liquid gradient within the sample averaged over the first temporal resolution interval as well as the influence of the meniscus both of liquid on the sides of the vessel as well as expectedly primarily on the sides of the sample. Should extremely accurate resolution within this minor region above the liquid surface be desired then hydrophobization

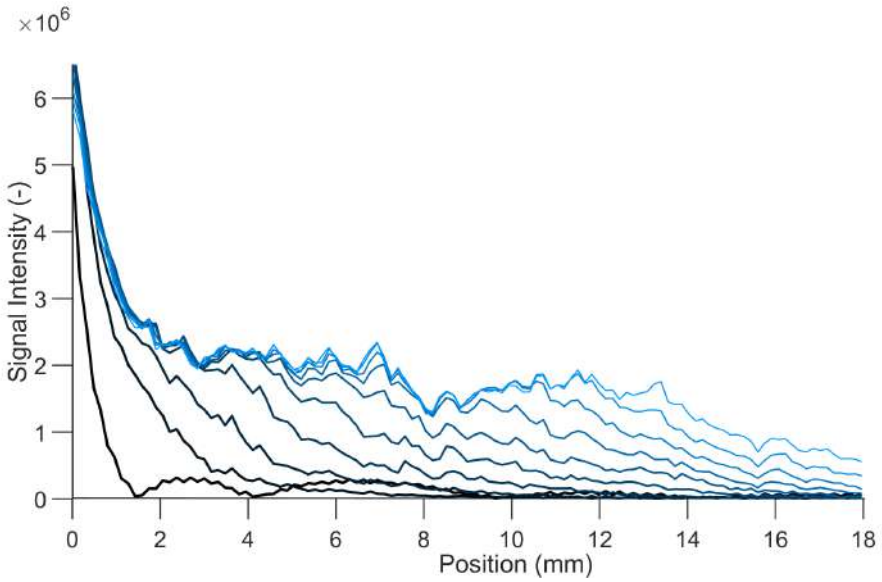


**Figure 6.1:** Edge-wicking results for hydrophilic egg-carton material through time in the form of signal intensity as a measure of liquid fraction in the egg carton sample from the liquid surface at position 0mm up the exposed carton material to the material's top end at 18mm. Experimental time 2 minutes: sequential 12 second intervals extend progressively from the thicker black lines to thin blue lines.

of the edges of the liquid vessel is recommended in order to invert the meniscus on the vessel edges and isolate sample effects. This is however not required for this particular testing due to the relative length scales applicable.

As time progresses, this gradient extends steadily further up the sample length representing liquid transport vertically through the material and furthermore steadily increases in intensity. It can be seen that at, for example, 4mm above the liquid surface; the signal intensity of approximately $2.4 \times 10^{-06}$ appears to remain as a steady state liquid concentration through the subsequent time intervals which is achieved by the measurement averaging the liquid content between seconds 48 and 60 into the test. As time progresses, the steady state reached is seen to progress further up the sample until it reaches 12mm from the liquid surface at which time measurements presented in the figure are terminated. The acquisition time for this particular measurement allowed a 12 second temporal resolution and spatial resolution of 156$\mu$m. The apparent noise due to fluctuating signal intensities is in this case not entirely due to measurement noise or error but rather the very rough and in-homogeneous nature of the material as was seen in Figure 5.2. For this measurement on a fast and highly absorbing materials the signal to noise ratio at the 12 second temporal resolution is still high and thus further optimisation can easily be made to the temporal resolution and spatial resolution should this be desired. The work is not focused towards optimisation for this egg-carton but rather the packaging material samples.

Quantification of the MRI signal based liquid uptake seen in Figure 6.1 is possible

through correlation of MRI signal outputs to mass uptake evaluation over the experimental time frame. This correlation methodology can be as simple as normalisation of initial and final liquid mass to relevant signal intensities. The final liquid uptakes are calculated with reference to the atmospheric liquid mass content against a fully dried sample and the mass uptake after the experiment's completion respectively. In this manner the absolute signal intensity whose quantification is dependent on several factors within the measurement system (as will be further discussed) should not be a source of measurement error. This simple method's applicability for measurement is further made use of during consideration of through-plane testing as found discussed further in 6.5. Furthermore, the position of the rising liquid front can be quantified through the combination of experimental MRI testing and reference visual tests allowing for the tracking of visual reference liquid fronts within material. This is though correlating a material absorption fraction or moisture content with the presence of the visual liquid front. Figure 6.2 indicates the manner in which this mass uptake as well as visual liquid front rise can be quantified. The figure displays two time intervals from the results of 6.1 normalised to the test's specific atmospheric and post-experiment liquid mass reference frames within the first minute of the experiment.

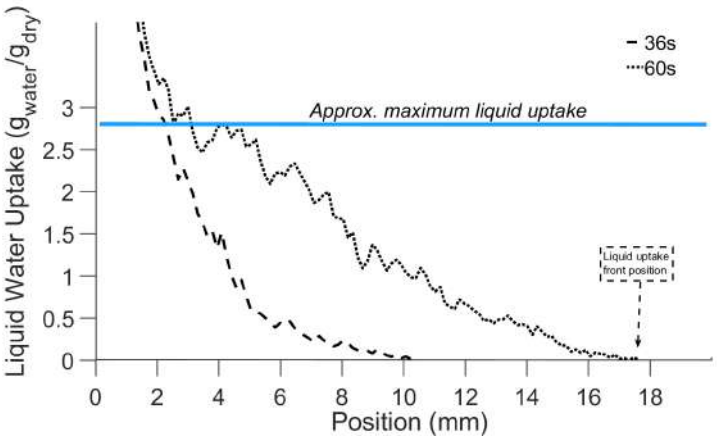


(a) Quantified MRI liquid uptake and front movement

(b) Moisture front visualisation: 60s

**Figure 6.2:** Edge-wicking results during liquid visual tests and visual liquid liquid front movement: Egg carton

It can be seen in the figure that during the first minute, approximately 6mm of the material is fully saturated. The first 2 mm of the sample above the liquid surface appear as over-saturated based on the figure but this is simply due to meniscus effects on the edge of the water sample penetrating the liquid surface. Considering the position of the initiation of liquid uptake in the figure (a) as correlated to the position of the visual front represented by the darker areas in figure (b) indicates how the initiation of moisture uptake correlates to the front position and this can be used to effectively track the moisture front. As the material absorbs further water, it expands and interacts with the absorbed liquid which leads to the signal quantity

increasing until saturation is reached.

This moisture front within the particular material is fairly inhomogeneous with minor variation in front and fingering of liquid fronts occuring. For this reason differences between experiments are possible within the particular material used not allowing for statement with full confidence whether the measured uptake aligns precisely with the visible liquid front. This result does however present a strong indication of their alignment and its material specific validity may be able to be more accurately assessed within more homogenous hydrophilic materials. The MRI measured front is however certainly not vapour phase as vapour is not visible within MRI measurements. The influence of vapour only becoming apparent upon adsorption to the fibres.

### 6.1.2 Sized materials in an open atmosphere

In-plane moisture transport measurement through edge-wicking experimentation was shown to allow for effective in-plane moisture front tracking and liquid uptake assessment using the MRI for highly absorbent hydrophilic materials. This same experimental testing is further implemented for sized sample materials.

#### Visual and bulk testing

Visual measurement of the position of a rising liquid front was experimentally conducted for the sized board material of sample B. In-plane water uptake as a process was explored to attain a visual reference useful in further MRI experimental testing.

For sized material B, visual tests conducted indicated the lack of in-plane water uptake of the material. Experiments were conducted both with reference to mass of liquid uptake as well as with inclusion of a liquid dye to more conclusively attain a visual liquid front indication. The addition of a liquid dye would to a degree alter liquid properties such as the liquid contact angle which would impact the edge-wicking extent. This is however not required to be further explored due to the similarity in outcomes attained in both the dyed and undyed visual tests. Results from such visual edge-wicking with coloured liquid are found in Figure 6.3.

Figure 6.3 displays a material B sample upon test initiation and after 24 hours after which time minor bulk liquid evaporation had occurred. It is evident in the figure that liquid uptake and retention does not occur to a visual extent due to the lack of movement of the waterfront over the experimental timeframe of 24 hours. Furthermore the mass increase of the sample was found to be consistent with no liquid uptake above the liquid surface. There is minor creepage up the edges of the material sample but no change within the central width area of the sample except for the visual effect of evaporation of the bulk liquid. This does not specifically conclude that in-plane moisture transport does not occur at all within the material, however the relationship between the liquid uptake and moisture loss due to evaporative effects from the sample is such that the liquid uptake and retention above the liquid interface does not appear to be significant. The liquid uptake, should it

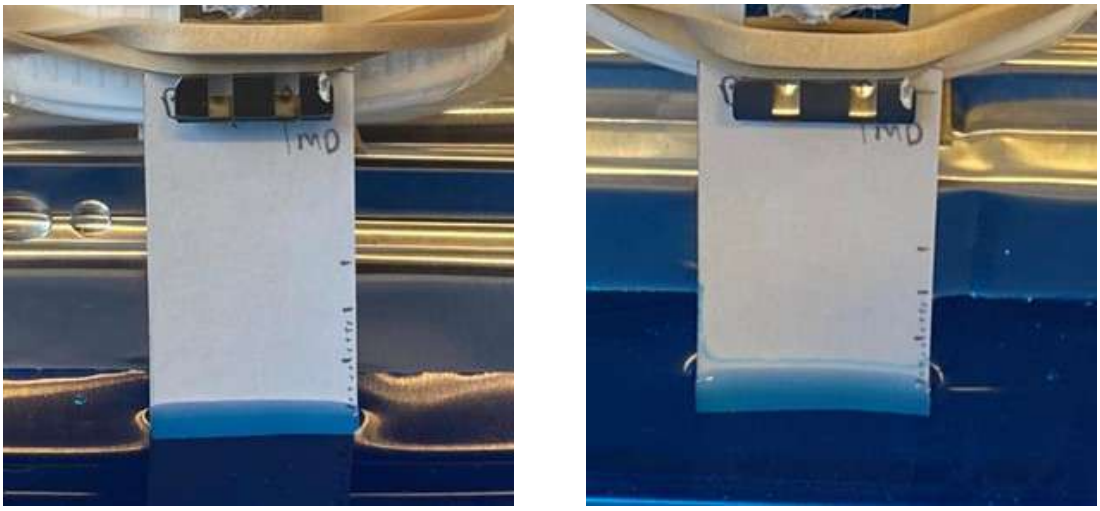

(a) Time: 0hrs (b) Time: 24hrs

**Figure 6.3:** Edge-wicking results during dyed liquid visual tests: Material B

be measureable within the MRI, is expected to take place through fibre diffusion as opposed to the inter-fibre capillary transport mechanism from 3.2.1 due to the sizing of the fibres altering the liquid's contact angle in the fibre pores.

A simple comparison between the liquid absorption rate when sample B is fully submerged in room temperature water to the rate of drying from initially fully saturated atmospheric material at approximately 22°C can suggest why this material does not take up notable liquid quantities above the liquid interface. This by indicating the high rate of evaporation. Figure 6.4 displays a baseline as to the relationship between material B's submerged moisture uptake rate and its open air drying rate for discussion of this evaporation rate.

The drying rate for the material under these atmospheric conditions can in Figure 6.4 be estimated to be almost linear at 0.014 grams of liquid per minute when fully exposed to the atmosphere for from the start of drying until approximately 90% of the initial saturated moisture content has been removed. This is compared to an initially extremely high uptake rate of $0.125\frac{g_{liq}}{min}$ for the first 5 minutes during which around 50% of the total liquid uptake occurs. This then transitions to a second slower absorption rate through which the final 25% of the liquid uptake occurs. The drying rate thereby becomes more significant than the liquid uptake rate for all but the very fast initial liquid uptake when the dry sample initially comes in contact with the liquid. The mechanisms and multiphysics behind such moisture uptake are not explored in further detail; however such uptake/drying relationships are provided as a reference baseline and further information on this topic can be found in [3]. What is indicated through this rate comparison is the high rate of moisture uptake required to retain more liquid within the material than is lost. It is seen in the results of the edge wicking tests that this high liquid uptake is not maintained above the liquid surface.

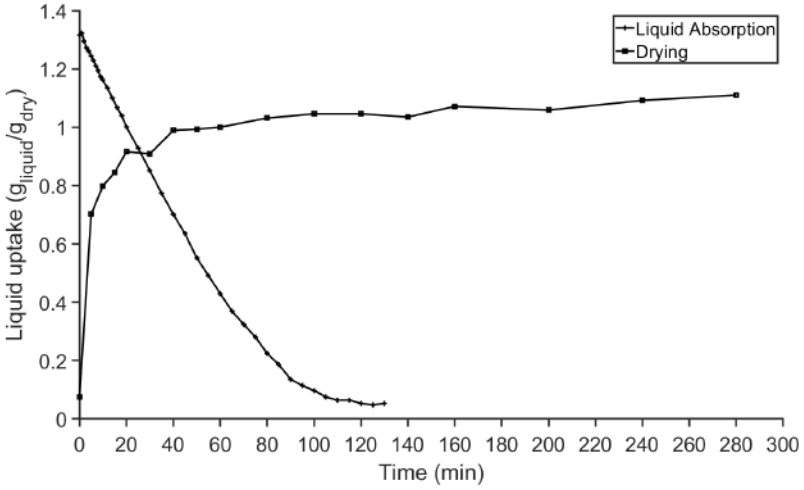


**Figure 6.4:** Comparison between the estimated liquid uptake and drying rates for material B

### MRI measurements of in-plane moisture transport for sized material

The visual edge-wicking testing on the sized sample materials provided a clear view of the apparent low sample B material liquid uptake vertically above the liquid surface within which the bottom of the edge-wicked sample is submerged. It was hypothesized that testing within the MRI may be able to shed light on potential liquid uptake not visually identifiable.

The lack of liquid uptake is however during the MRI testing procedure confirmed through the MRI material B sample area testing. The sample area above the material water surface does not indicate any sign of signal intensity fluctuation over time due to uptake as was indicated when edge-wicking the hydrophilic egg-carton material discussed above. This is displayed within the MRI results as displayed in Figure 6.5. In the figure, a smaller representative sample area of 4mm is considered in the plot due to expected lower material liquid uptake. The signal intensity at the 0mm position indicates the water surface and from it extends a smooth curve of decreasing signal intensity until approximately 2mm. From this point the signal intensity is negligible. What is seen here is the effects of the meniscus discussed before with in this case the curve likely stemming for this hydrophobic material from the manner in which the rig operates. The water carrier in which water is contained is threaded up from the bottom at the test's initiation as seen in Figure 5.8. Once it reaches the top it slips marginally down into a notch approximately the depth of this seen profile's height for stability and consistency in positioning. The liquid surface thus is to this marginal degree above the final liquid surface position for a minor period as the liquid holding cup reaches the top of the threading of the rig before this liquid cup drops down into the notch cup locking mechanism. Liquid appears to due to surface tension remain on the sample surface forming the visible meniscus in this case. No liquid uptake can be seen in the figure. From the initial time point until the 12 hour mark the only change in the liquid representative signal curves is the change in the

liquid's surface position as a result of evaporation from the open experimental setup.

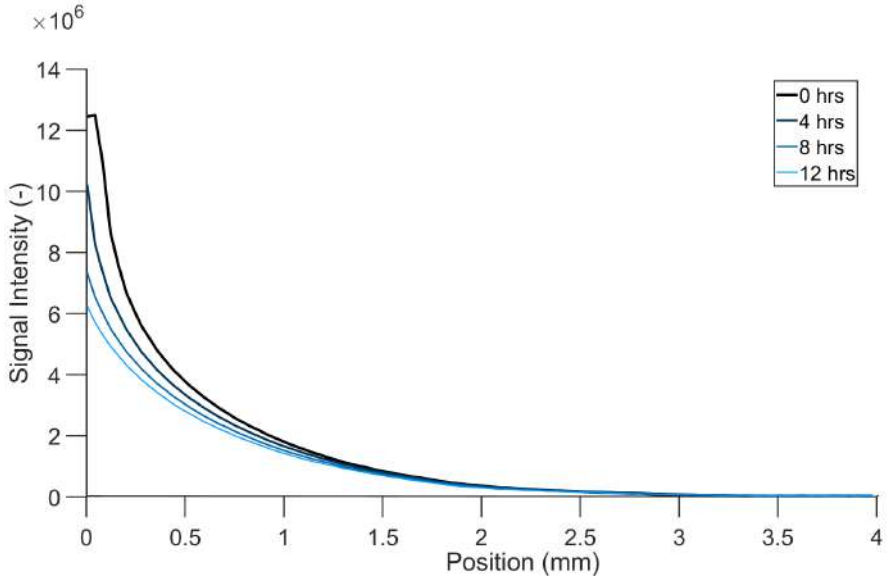


**Figure 6.5:** Edge-wicking results for material B

A number of signal optimisation strategies were used during testing in order to extract signal from possible liquid uptake. During this represented testing in Figure 6.5, an MRI imaging sequence based off of effectively implemented sequences from the Cobb styled testing in which liquid uptake was measured within the sample were deemed appropriate and thus it can be concluded that the lack of signal is due to lack of measurable liquid content within the sample and not lack of an appropriate MRI imaging setup.

Both visual as well as MRI testing here thus indicate a negligible extent of moisture uptake and retention above the liquid surface.

### 6.1.3 Liquid uptake from a contained atmosphere

Inplane transport measurements through edge-wicking testing could be conducted on these materials in a closed, contained setup. When contrasted to the testing in an open environment, testing in this fashion minimises the effect of material drying through evaporation by allowing the system to reach a state of humidity saturation as well as introducing material liquid uptake from a humid atmosphere. In a similar fashion to the open air edge-wicking, no indication of liquid uptake is visible during an 8 hour experiment at identical MRI settings with which moisture uptake was viewed during through-plane testing experiments as will be further dicussed.

As would be expected from this contained edge-wicking test on material B; a liquid uptake test from a closed and moisture saturated atmosphere without direct liquid contact does not indicate any interpretable response but rather only 'noise.' This however does raise an interesting observation to note as by weight, the raw

atmospheric uptake test measured a liquid uptake fraction up to 40% of the total submerged liquid mass uptake. The contained edge-wicking experimental test measured similar liquid mass uptake if the submerged portion of the sample is excluded.

As these mass uptakes from contained atmosphere edge wicking and contained atmosphere vapour moisture uptake with no liquid contact are significant and no signal was received, the question needs to be posed in what form this liquid uptake occurs and why this cannot be seen during the testing. This, when compared to the through-thickness testing results still to be presented in which liquid uptake is visible, would give an indication that the liquid populations may not be the same between these two liquid uptakes. Further work in this area would be interesting to consider.

These presented results do display a potential future application for MRI use in the study of paper material liquid uptake. Work has however been conducted to an extent in the vapour uptake of dry paper samples by various authors. For this reason focus is in this case is not set in vapour liquid uptake but rather focus is put towards studying of the through-thickness liquid uptake testing methodology of similar form to the Cobb testing methodology often made use of in the characterisation of sized materials.

## 6.2 Through-thickness moisture transport

A Cobb test is generally conducted over a time-frame of 60 or 180 seconds. As discussed further in Appendix B, temporal resolution of approximately 1 minute was found to be near the upper limit allowing for acceptable signal to noise ratios based on findings discussed in section 6.3 and for this reason analysis is considered over longer time frames.

Results obtained come in the form of a signal intensity (related to water content) plot with positions extending vertically from a position which is within the higher signal intensity water region above the sample, through the sample region to below the sample region within rig supportive material. Such signal profiles can be attained sequentially to obtain a signal profiles through time as is presented in Figure 6.6. It is the sample through thickness region, referred to as the area of interest (AOI) which is to be analysed further.

## 6.3 Experimental validation discussion

In order to attain practical results, one must be certain that signal is attained within the area of interest and that the signal for analysis stems from sample responses. Due to the small length scales across the sample's through-thickness as well as the significant signal discontinuity between liquid water and dry samples this is espe-

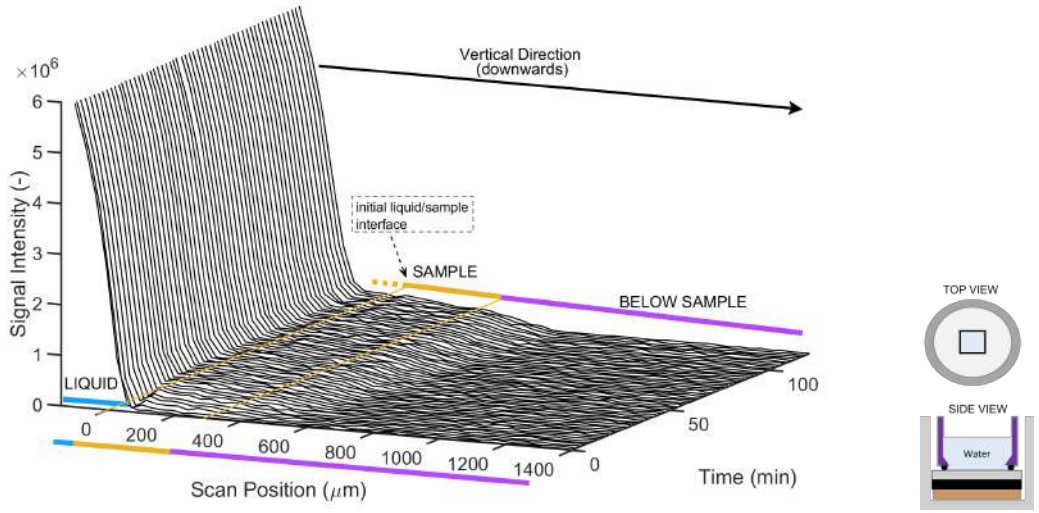


(a) Signal profile (b) Rig

**Figure 6.6:** General Cobb styled signal profile visualisation

cially important in this work. Initial work in this regard is discussed for reference in Appendix A as the experimental rig is designed to achieve realistic optimised signal profiles. In this sense validation is conducted both with regards to verification of the signal's presence, origin as well as assessing potential alternate signal sources to be aware of during experimentation and testing. MRI imaging considerations as well as further validation is also found in Appendix B for further reference as to MRI settings choices.

An initial validation of whether an uptake in liquid over time occurs and is measurable is presented in Figure 6.7 displaying the signal attained across an interest region within which the sample is located. The experiment has an image acquisition time of approximately 2 minutes and the AOI extends from the measured water surface contacting the sample's top face through its thickness and beyond. Free water presents a much higher signal than the water bound within the sample and thus the drop-off within the plots represent the transition point between free water and sample. The MRI imaging settings and resolutions are discussed further through the text as well as in Appendix B.

The figure visualises a signal response attained through experimental time below the water face and that as such uptake of liquid is measurable. The water face does marginally change position over time due to effects such as sample expansion and buckling which will be further discussed. The area in which liquid uptake is measured however extends over an area larger than the 360$\mu$m thickness of the sample to around 600$\mu$m below the liquid surface even though the sample has a fixed base position and thus liquid measured below the material area stems from below the fixed sample. For this reason consideration is made as to the source of this signal before absorption dynamics are analysed.

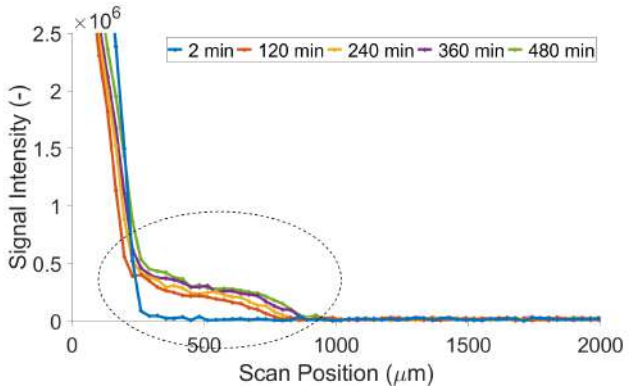


(a) Larger field of view overview over the measurement area

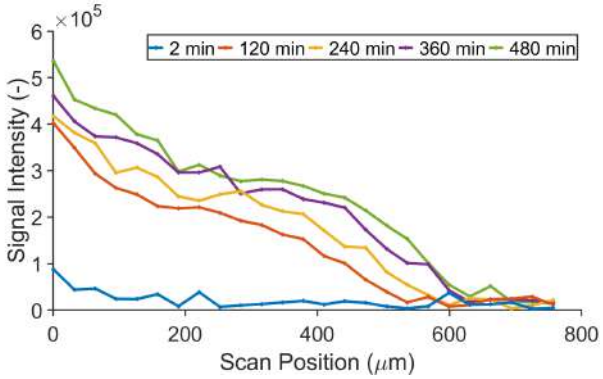


(b) Close up within the circled area of interest (AOI) within plot (a)

**Figure 6.7:** Material B validation of liquid uptake measurement at different time points

### 6.3.1 Signal response from the rig

With the rig's construction being from sintered nylon and resin and the rubber set above the sample being a rubber compound, there exists the potential for signal stemming from these sources conflicting with signal attained from the sample itself. The signal attained from isolating the signal of the dry rig is found in Figure 6.8. The scan position runs from a position within the rubber material against the y axis which is experimentally above any sample through to the plastic rig base experimentally below any sample. The signal was isolated by running an experiment in a completely dry environment without the influence of the free water present during general testing runs. In the figure two tests are presented, one running without a paper material sample within the rig and one with such a sample present. Both signal curves have high noise and low absolute signals due to the lack of water presence.

Signal is seen to stem from the dry rubber to a greater extent than the dry plastic material of the rig. This could be the influence of aromatic groups or other liquid compounds within the rubber material. Signal within the rubber is not significant in comparison to signal stemming from water within the rubber's central square hole (refer to Figure 5.10) which is an order of magnitude larger and thus

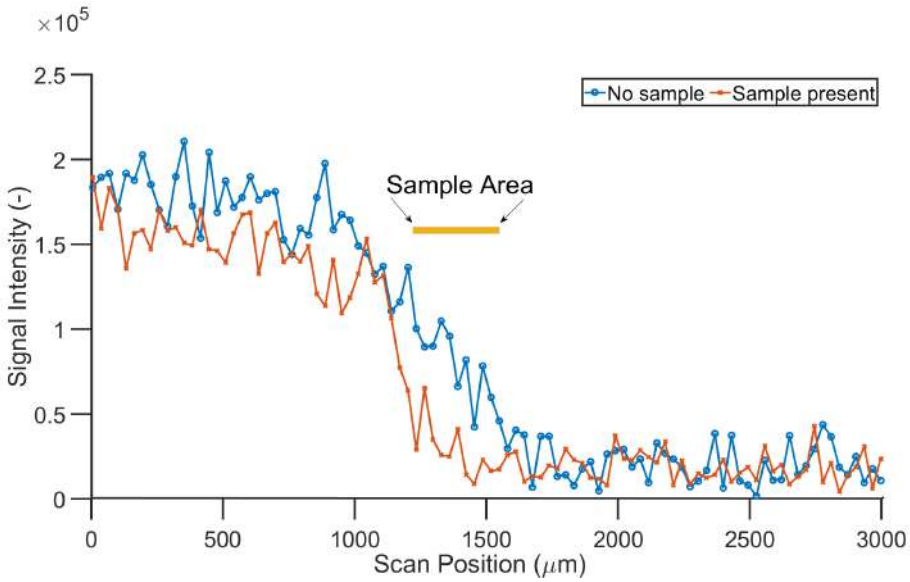


**Figure 6.8:** Visual indication of the signal stemming from the dry sample rig while in a test setup with no water present. The two presented experiments omit and include a sample respectively.

this effect is acknowledged but will not impact results. The signal stemming from the dry rig base is noise and thus its effect negligible.

Within the transition between these two materials lies in one case an atmospherically dry sample ($\sim 7wt\%$ moisture content) and in the other no sample. The positioning of the rig base bottom is consistent and due to this the position of the signal stemming from the rubber should be expected to be raised by the thickness of the sample. This is found to be the case in Figure 6.8 and the position of the sample can be inferred. The atmospherically dry sample's signal is in this way found to be comparable to the signal attained from the rig's dry plastic.

During the course of an experiment, water passes through sample and is able to come into contact with the originally dry plastic base. The influence of this liquid contact with the base during experimentation can be seen in Figure 6.9. Here a similar experimental comparison is made to before, however the rig's partially rough surface and the rubber have both been in contact with liquid in the prior experimental run before being wiped dry for the subsequent testing. Contact with this liquid through a sample material is representative of conditions experienced during testing over longer time intervals.

In the figure it can be seen that liquid not only remains within the plastic rig base surface, but additionally to a lesser extent on the rubber surface. Signal stemming from the rubber is expected to be found within minor printing imperfections that are visible, but the signal can be neglected as the rubber's signal was neglected before. The plastic base appeared dry to the touch in the dry sample test confirming the liquids presence within surface grooves and pores of the 3D printed plastic. For

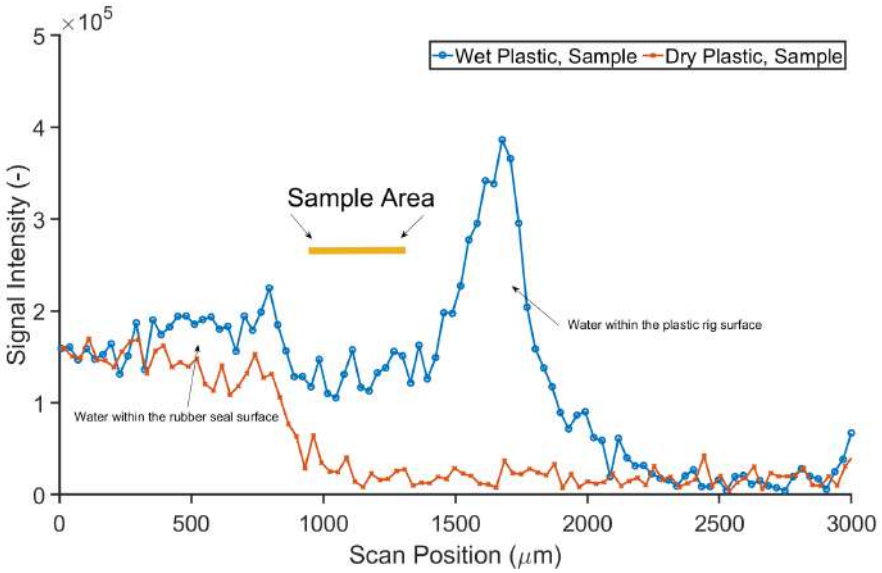


**Figure 6.9:** Visual indication of the signal stemming from the sample rig while in a test setup with no water present but that has been in contact with water and wiped dry. The two presented experiments omit and include an atmospherically dry sample respectively.

this reason signal arising within testing results in an area below the expected AOI can be neglected and attributed to this source. A comparison of this wet plastic base signal to signal obtained below a sample during an experiment does confirm this signal attribution explaining the artefact seen within Figure 6.7

The symmetrical triangular profile of the liquid within the wet plastic sample seen in Figure 6.9's blue curve have two possible sources. This could be attributed to either the nature of how the liquid is physically contained within groves of the structure, or else attributed to the water lying as a flat and consistent single layer of liquid on the rig base viewed from a slanted angle due to the improper angle of the rig base. This improper angle in comparison to a perfectly side on through-thickness profile view. Such a misalignment of the experimental setup would lead to inconsistent results with a lack of valid signal profiles. In this case the symmetrical profile of this liquid is believed to be due to the former alternative, this being the liquid's positioning within the material concluded based off of the learnings discussed in appendix A. No notably significant experimental error from such experimental positioning is expected to harm experimental conclusions.

An important learning from the presence of liquid within the sample base support unit of the rig is the requirement to use an entirely dry sample rig base (not just dry to the touch) during testing. Within Figure 6.9 the signal obtained from within the initially dry material appears higher than when the rig was dry to start. This is expected to be due to minor liquid uptake from the 'wet' rubber and sample base support during the sample preparation and insertion process which can take several minutes and expected to skew results should a rig plastic base containing

liquid be used.

Signal attained within the sample is able to be considered as 'noise' due to its low intensity as is seen through the consistency between signal stemming from the dry plastic supporting rig and the sample area in the figure. At initiation of an experiment the sample itself has an atmospheric moisture content. This initial moisture content, of approximately 7wt% within the relevant experimental environment, is considered the natural baseline and due to the general climate consistency through control present within the MRI housing room not considered to fluctuate to levels which would disturb any experimental results. Housing of samples within sealed plastic housings until extraction for experimentation only improves upon this consistent initial moisture content. This baseline can however be perceived as a limit to the experimental measurement of liquid content within the sample material as corroborated by literature.

### 6.3.2 Repeatability

Validation of the experimental method repeatability can be conducted with independent experimental runs achieving very similar signal intensities across difference measurement slices and across independent tests. An exemplar of such a validation is presented in Figure 6.10 which displays an increase in moisture content (seen through signal intensity) through time over three independent tests at these same conditions. The exact dynamics are not able to be seen in this plot due to its positioning, however general comparative trends are to be focused on in this assessment. Measurements are shown at three of the ten independent points through the sample thickness. These thus consider the sample paper's position as the area of interest (AOI). This area is through visualised through a selection of figures presenting the moisture content within a specific sample area measured with time.

Within Figure 6.10 it is evident at first assessment the differing moisture uptake profiles between different layers of the material. Near the material surface moisture uptake is initially rapid before a slower steady uptake after roughly 10 minutes. This initially accelerated moisture absorption however tails off through the material's thickness to this initially rapid uptake not being immediately evident nearer the bottom of the through-thickness. Comparison of the moisture uptake curves from 6.10 visualise the reproducible nature of the experimental methodology. Differences between the moisture contents of after 1 hour of absorption range between from 15 to a high of 20% in the upper half of the material while this can extend to up to 25% nearer the material's lower surface. This reproducibility of this result, notably contrasted to individual experimental noise adjustment estimates of up to 10% is considered sufficient.

#### Material buckling

Note is to be made of the effect buckling has on the experimental results. Within the experimental rig, the circular sample is constrained with a square sample area

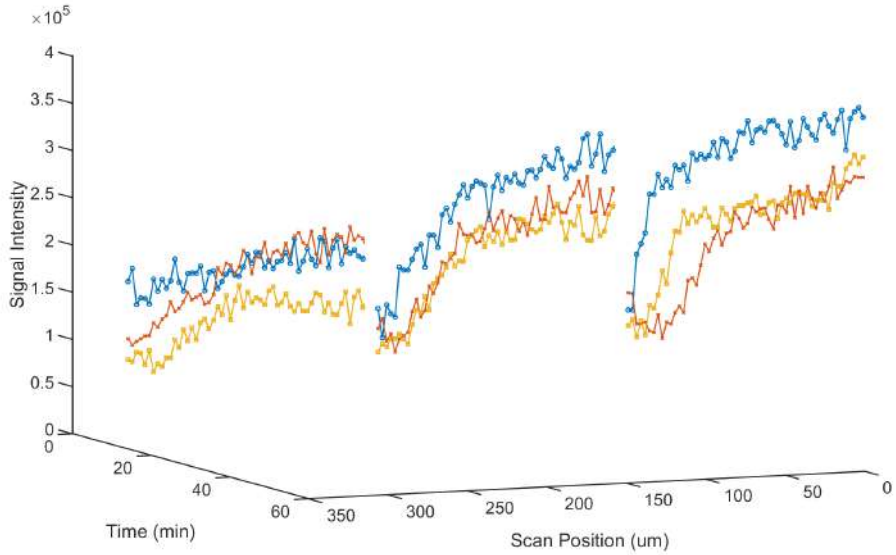


**Figure 6.10:** Exemplar material B2 validation: test 1 (blue), test 2 (orange) and test 3 (yellow) represent three independent experiments at corresponding positions through the thickness of the paper. Scan position 0$\mu$m representing the area of the top material face through the middle to the lower end of the through-thickness at 350$\mu$m.

exposed to the liquid comprising approximately 10% of the total sample surface. Paper as a cellulosic fibre material naturally expands upon absorption of water as discussed in 5.2 but the water tight constraint applied on the edge of the exposed sample area does not allow for material expansion across this boundary. For this reason; as expansion of the sample takes place, material buckling occurs within the measurement zone. Buckling effects become visible after approximately 5 minutes and stabilize after 25 minutes as is indicated by Figure 6.11. Here the white block represents a side profile of the square water profile laying above the through thickness of the sample with the vertical direction of Figure 5.10 extending from top to bottom of each subfigure. The dark shadow ingressing into this liquid block from the bottom indicates the change in position of this buckling material. In Figure 6.10, the buckling pattern of the test 1 runs parallel to the MRI measurement direction, similar to the buckling seen in Figure 6.11 while tests 2 and 3 buckle in a perpendicular fashion. Such buckling is an unavoidable result owing to the hygroexpansion of the material.

Further validation of the experimental measurements is attained through measurements not impacted by this dynamic buckling. Figure 6.12 shows the moisture absorbed by the sample in an area not exposed to liquid water and thus any absorption occurs due to radial liquid transport. Here, in an area with highly restricted expansion, the consistency of the experimental results are most evident with differences within the middle and lower region of the sample through-thickness being due to initial measurement error rather than absorption differences. The impact of the compression is not discussed further in this context as these results are presented as

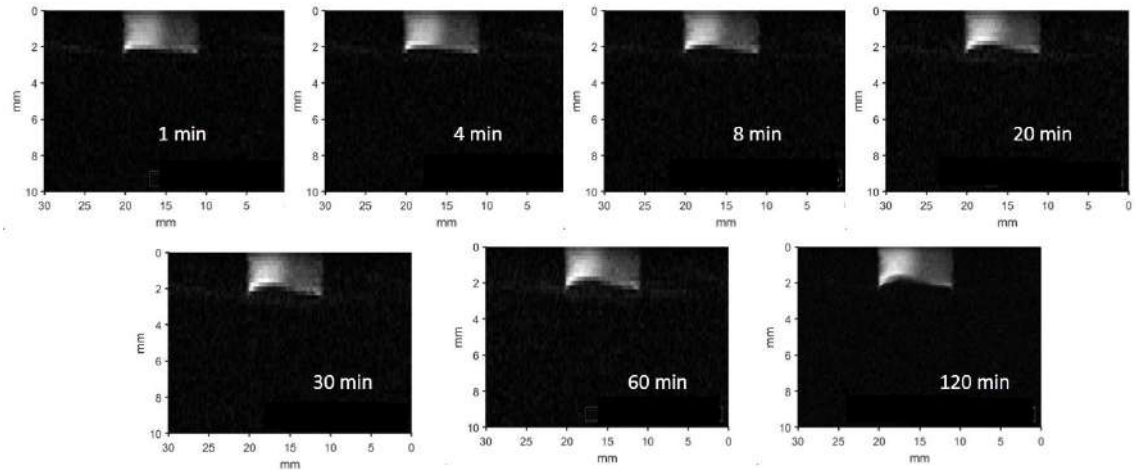


**Figure 6.11:** Visual progression of the buckling of a sample

representative. Buckling is seen to impact experimental results, however its effects do not take from their applicability.

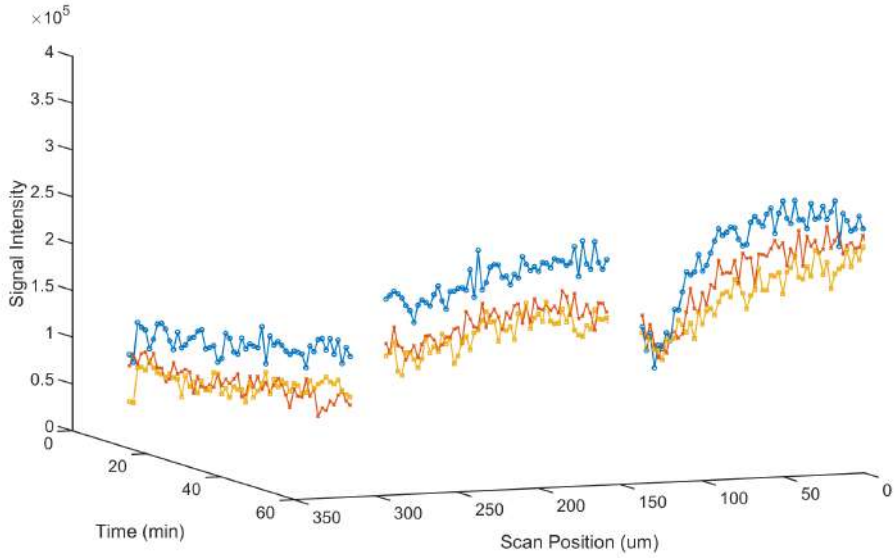


**Figure 6.12:** Exemplar material B2 validation in a compressed non-buckling area: test 1 (blue), test 2 (orange) and test 3 (yellow) represent three independent experiments at corresponding positions through the thickness of the paper. Scan position 0$\mu$m representing the area of the top material face through the middle to the lower end of the through-thickness at 350$\mu$m.

In an attempt to reduce the possibility of buckling, the size of the liquid contact area was reduced from $1cm^2$ to $0.25cm^2$. In this way it was expected that expansion forces would be localised and buckling would be less significant as the sample would expand as a single region rather than folding and buckling. This was indeed the case, however results from such an experiment are less valuable due to the reduction in signal quantity as discussed further with reference to slice thicknesses in B. It is

more appropriate to increase water contact area than decrease it. This is presented as a further design approach recommended in further experimentation.

Buckling takes place within the experimental rig directionally perpendicular to square sides of the rig rubber seal internal opening. The directionality of the buckling does not in this case appear to be entirely predictable and could be either parallel to or perpendicular to the MRI imaging slice. It is hypothesized that the directionality of the buckling in fact be consistent and predictable due to the well known differences in mechanical strength as well as expansion rates between the directions, this however does not appear to be the case. The specific directionality of the externally attained sample paper is however unknown neither to the experimenter nor the sample material's source. The direction of buckling expectedly has an effect on the profile of the absolute signal response above the known material surface dependant buckling direction. For this reason expansion above the initial liquid/material interface is not considered within these measurements and thus only the area within which material is known to be at all times independent of buckling orientation.

The buckling shape, visualised through Figure 6.11, is however again not detrimentally critical to the moisture measurements as measurements are taken over an averaged $1cm^2$ area of the material at each positional point which is consistent across all samples and thus is representative of the buckling (which is consistent in shape even if not in direction) no matter the buckling direction. In this way absolute material buckling effects deviation from within the AOI measurement zones is consistent. Figure 6.13 provides a visualisation of how the total signal quantity is consistent despite buckling direction knowing that buckling shape is consistent. Green is considered the material area from which the MRI measurement signal is attained within which the material is 'unbuckled' while the white area is area in which buckling plays a role in the signal achieved. Total signal measured by the MRI, as the liquid contact area is across the entire individual squares, is represented by the summed area of green colour and white colour within the plot. This would be a representation of a single 'measurement height' slice across a certain position of the sample's through thickness from a top down view with multiple of these height slices taken through the sample. Despite the direction, the summed area of each of these representative slices is representative of signal measurable in both the influenced and uninfluenced areas is generally consistent across both orientations. For this reason buckling is a phenomena considered to be consistent phenomena across tests.

### MRI signal

Signal achieved from the MRI is attained through a complicated set of calibration functions, magnetic field shimming and reference normalising that is conducted by the MRI before the raw signal is recorded upon which Fourier transforms can be conducted and the output interpreted. A simple example of one of these reference systems could be the 'receiver gain' of the system which is automatically optimised by the system and has a non-linear relationship with absolute signal output. In this

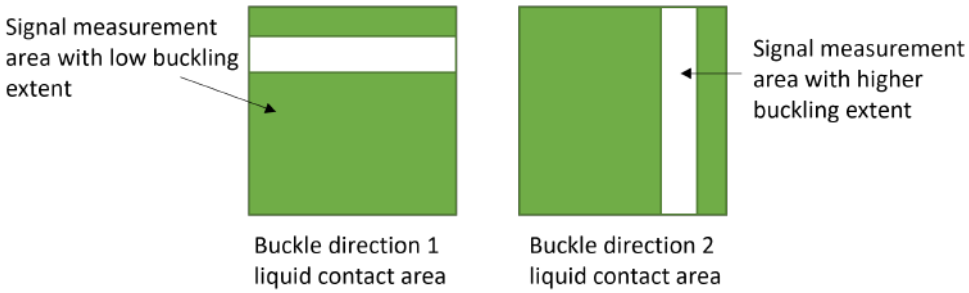


**Figure 6.13:** Visualisation of how buckling direction does not detrimentally impact result outcomes knowing that buckling direction is consistent and signal is attained from an averaging of the entire area at each vertical position.

way, should a system optimisation be conducted within the system and come out slightly differently between two 'almost' identical experiments, the signal outputs would not be linearly scalable and comparable to each other. This has not caused any known problems in the experiments conducted but, due to the time limitations on this work however, a full detailed understanding and review of the extremely complex systems made use of within the MRI background systems is not attainable and thus potentials for other such unknown sources of background process signal deviation cannot be ruled out by the authors. Furthermore, simple differences in vertical positioning of a sample within the measurement area can lead to discrepancies between signal datasets. This is due to the averaging of signal quantities over the appropriately defined measurement zone. An exemplar hypothetical visualisation (representing the experimental rig as per Figure 5.10) is presented in Figure 6.14 where the slice averaged over taken over the entire representative purple block area area on the left from a top view is positioned vertically in two different areas comprising fields of view over different material majorities on the right.

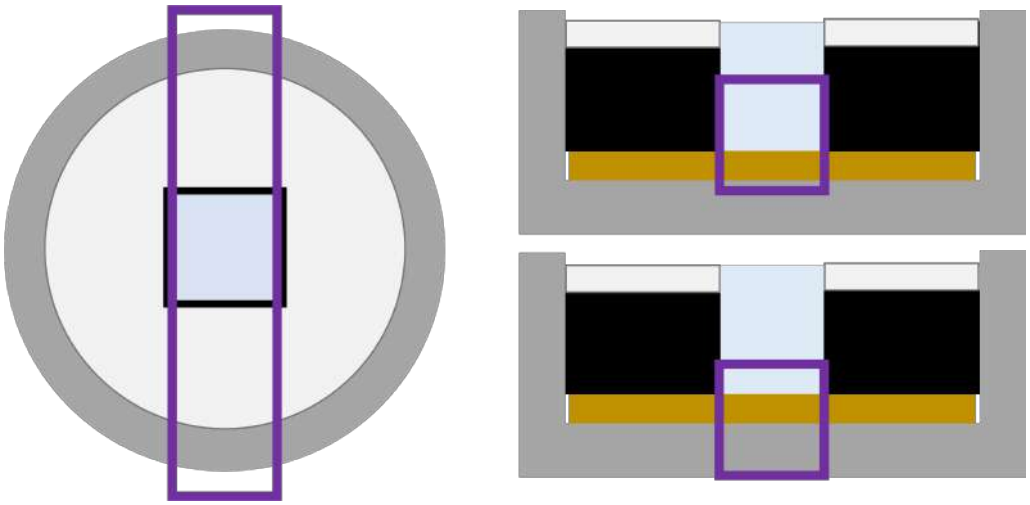

**Figure 6.14:** Exemplar visualisation of the sample measurement slice from a top and side view between two vertical field of view positionings

In the figure two identical experiments are conducted with the difference being only the vertical position of the sample and thus the amount of water present within the entire vertical field of view. Measurements per height position are taken independently through the vertical resolution, however in this example two different signal intensity maximums may be attained due to the experimental slices having a greater total fractions of water within the measurement areas. Signal normalisation can thus be applied to the signal intensity measurements

**Signal normalisation**

Overall the experimental error from the accumulated effects of the material buckling, the slight positioning differences and other small changes can, on the length scales applicable to this form of testing, lead to deviations notably larger than what was presented within the prior comparisons in experimental results. Deviations such as these when considering raw signal intensities cannot be discounted, nor can differences such as these allow for comparison between different material types as no consistent reference curve for a particular material can be constructed in confidence. The differences are however majorly in the absolute signal quantity attained rather than the relative rates of signal (and thus moisture) change within the material through time. The initial moisture fraction of the samples tested as well as the final moisture contents are measurably consistent through testing, and it is thus known that the experiments are consistent in their essence despite how absolute signal intensities may appear to contradict this.

The same overall sample liquid mass uptakes over the time frame thus despite different absolute signal intensities describe the same overall sample moisture contents. The signal intensity should for this reason not be seen as a tool for direct comparison between different tests. This signal can however for visual consistency be normalised between initial and final moisture contents and analysed with a more representative plot similar to that of 6.10 is seen in 6.15 plot (a) in which a comparative initial view of significant deviation between tests n the same material is seen.

This is not a solution which removes error from experiments but rather a manner in which error can be acknowledged and the essence of the data's rates visualised simply. It is through this means seen that the experimental rate shapes are comparable when normalised which bodes well for the experiments' consistency in fundamental nature. Figure 6.15 plot (b) shows how this normalisation gives an idea that the outcome of the experiments have similar profiles over time and can be seen to be describing the similar overall liquid uptake rate profiles through time. What can however not be seen is whether any gradients exist within the sample itself. The experimental rig's central square liquid contact area allows a restricted liquid contact area through which liquid enters the material. From here however the liquid spreads radially through the sample. This liquid spread can however not be measured through the MRI with the current experimental methods. For this reason it is not known whether a gradient exists through the sample radiating from centrally within the sample or whether the moisture content through the sample is consistent. It is known from Figure 6.4 that the absolute liquid uptake within an

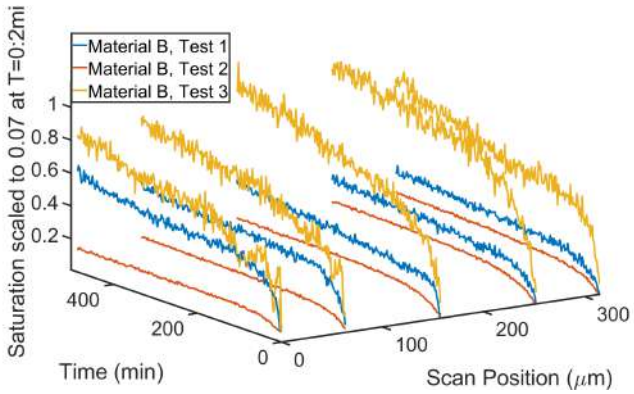


(a) Non-normalised signal

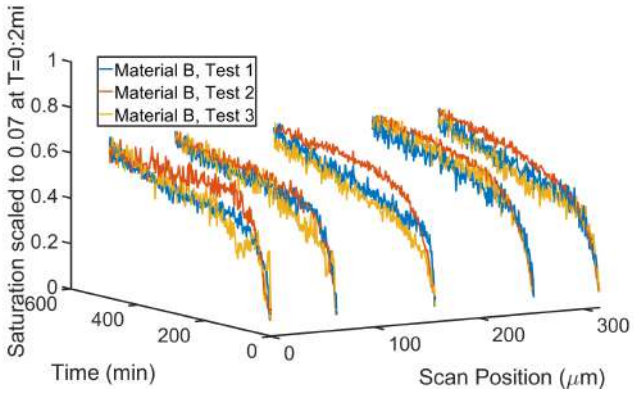


(b) Normalised signal to liquid uptake

**Figure 6.15:** Normalised signal compared to non-normalised signal profiles

entirely submerged sample has a liquid uptake of approximately 1.3 grams of liquid taken up per gram of dry sample and it is known that the liquid uptake after 8 hours in the Cobb style experimental rig is only 0.7 $g\frac{g_{liq}}{g_{drysample}}$ which is significantly less.

In order to not smooth over the potential gradients, it is not applicable to normalise the curves to a liquid content both initially and after the conclusion of the experiment as this normalisation would have no fundamental basis behind it. The normalisation is for broad view comparative purposes and further analysis will not make use of this normalisation but rather a normalisation to a standard atmospheric initial liquid content only.

### 6.3.3 Liquid uptake of material B

Optimisation of MRI imaging settings is an important aspect of MRI analysis as this allows for the best possible signal to noise ratios, spatial and temporal resolution optimisation and total signal quantity for use in results analysis. Work in this regard is found as per Appendix B, and the optimised imaging settings are presented in Table 6.1.

| FOV | Slice Thickness | Points | TR | TE | Averages |
|---|---|---|---|---|---|
| 4mm | 1cm | 128 | 2000ms | 6.064ms | 8/32/64 |

**Table 6.1:** Coatings comparison: MRI imaging specifications for 60 min tests

The highest potential temporal resolution is approximately 15 seconds corresponding to imaging using 8 averages at the consistent MRI. The high 15 second temporal resolution would be desired to allow for imaging of the material buckling processes which occur within the initial minutes of the experiment as well as to attain clearer data within the initial time period within which the liquid uptake rate is expected to be more rapid. Longer temporal resolutions of 32 and 64 averages with temporal resolutions of 1 minute and 2 minutes are expected to allow for higher quality data over longer time periods and combinations of these temporal resolutions would be able to provide accurate descriptions of liquid uptake through all phases of liquid uptake.

Analysis of the moisture uptake for material B is considered initially over a 60 minute time-frame, this being in essence an order of magnitude longer than the typically used Cobb60 test. The uptake in 60 minutes will initially be analysed with reference to the signal response attained from the MRI.

Despite this uptake being over a comparatively long time-scale, the liquid uptake is surprisingly seen to follow a relatively linear rate through three independent points through the sample thickness in Figure 6.16 (a). This conclusion is not in line with expectations of the material and thus should be treated with scepticism. With a temporal resolution of 15 seconds corresponding to imaging with 8 averages, this is unable to account in detail influence of sample buckling as was seen in Figure 6.11 and other faster processes nor does it have a good signal-to-noise with noise in these measurements, although being apparently distinguishable from the overall trend, being high. Experimentation at this high signal-to-noise ratio was conducted to allow consideration of the first ten minutes and thus allow consideration of the period of buckling with more detail. The results of this experiment as displayed in plot (b) of the figure do not aid in the description of liquid uptake dynamics within this period. Nearest the material surface, at AOI position 0$\mu$m, an initial increase over and above that of positions further into the sample thickness is seen which can likely be attributed to the buckling phenomenon. This could be due to free water intrusion into the surface as it begins to fold before the overall expansion re-filling this area at around 10 minutes after which the linear liquid uptake resumes. There furthermore appears to be a decreasing liquid content gradient extending through the sample through-thickness from the liquid contact surface to the sample base in the figure (a). Such artefacts cannot however be validated and thus will not be explored further nor will the apparently linear liquid uptake rate. The noise at this temporal resolution is too high to accurately derive conclusions from the outcomes and thus this temporal resolution is not applicable as a measurement tool.

Due to the low signal to noise ratio at short temporal resolution, a higher num-

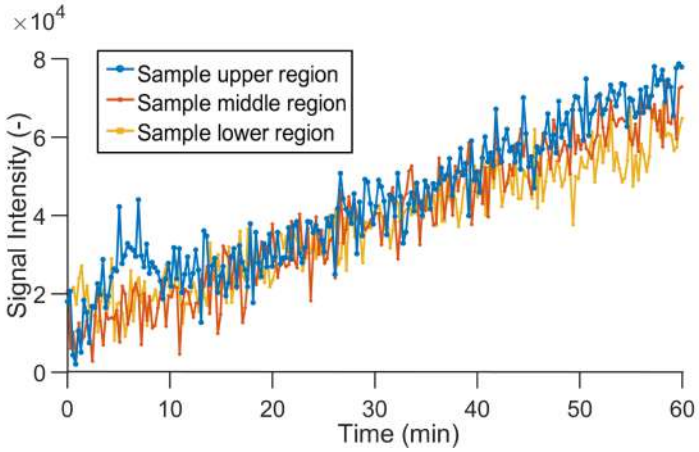


(a) 1 hour's uptake at 15s temporal resolution

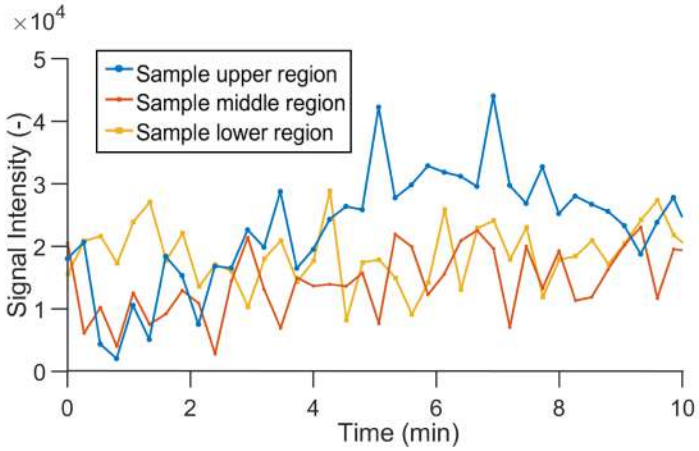


(b) Initial 10 minutes

**Figure 6.16:** AOI liquid uptake: 8 averages 60 mins

ber of averages allows for longer acquisition time and thus a higher signal uptake. An experiment with 32 averages will attain 4 times more signal than one with 8 averages and one with 64 averages double the signal of 32. The acquisition times of course follow suit. In Figure 6.17 this is not quite as clear due to the discussion regarding signal acquisition, however what can be seen is how the results of the 32 averages and that of the 64 averages tests are able to quantify the moisture content gradient between the lower and upper regions more effectively. The initial minutes of the 32 averages test is hampered to a degree by a slightly wet rig, however the improvement in attainable and interpretable data as the temporal resolution is lowered is evident over the first 60 minutes of liquid uptake. Most evident in comparison of these results is the emergence of a more defined indication of the presence of a liquid gradient in the through-thickness direction from the material upper surface closer to the liquid surface down the the material base. This appears significantly more defined in the test with a slower and higher quality signal intensity.

It is clear within Figure 6.17 that within the first 60 minutes of liquid uptake the

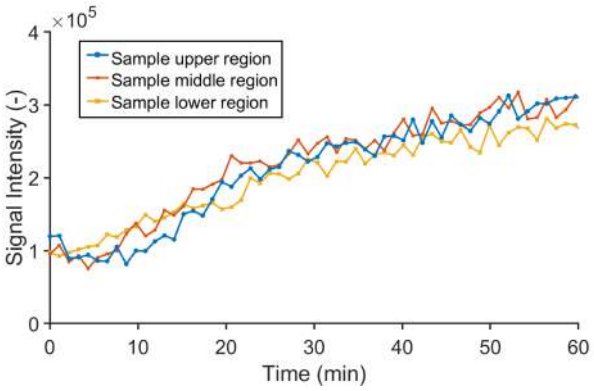


(a) 32 averages 1 min temporal resolution

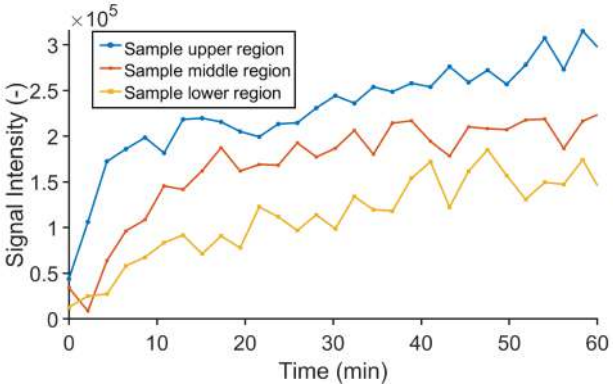


(b) 64 averages 2 min temporal resolution

**Figure 6.17:** AOI liquid uptake: 32 and 64 avgs: 60 mins

rate of absorption does not reach a point indicative of liquid saturation and for this reason experimentation over longer time-frames is appropriate despite this already being a time-scale not comparative to the Cobb60 test. Liquid uptake for the lesser hydrophobized material B has thus been found to be appropriate to analyse not on time scales of seconds as is typically done for Cobb60 tests but more appropriately over minutes and hours. The most appropriate temporal resolution on which analysis can take place is a two minute acquisition time and thus further analysis will take place at this temporal resolution.

An experiment conducted over a time period longer than this first hour can be found in Figure 6.18 which displays the water uptake over an 8 hour period with a temporal resolution of 2 minutes corresponding to 64 averages from material B test 1.

Should the initial period of the absorption be reconsidered at this lower temporal resolution, it is apparent that more data is able to be extracted from it due to the reduction in signal noise and relative liquid absorption rate relationship when comparing initial and final absorption rates. Within the initial 20 minutes of experimentation there is an high moisture uptake rate before a transition period to a slower, almost linear liquid uptake regime. Within the initial liquid uptake the possible three mechanisms discussed in 3.2.1 are expected to drive moisture uptake

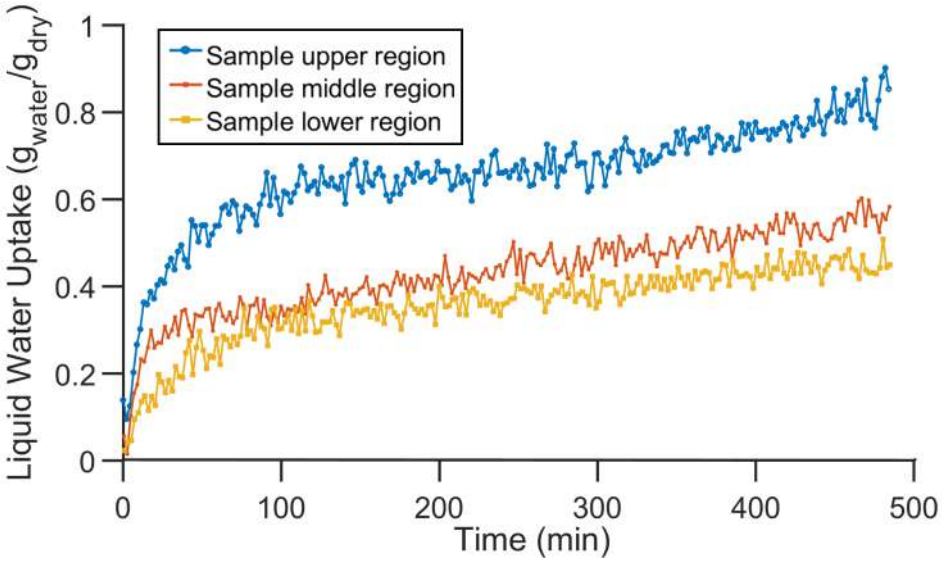


**Figure 6.18:** AOI liquid uptake: 64avgs: 8hrs (Test 1 material B)

while within the latter slow regime it is expected that the uptake is due rather to changes in the cellulose structure of an already saturated material that allow for increased uptake. This change thus gives the impression of a change in dominant liquid uptake mechanisms between the initial and latter rates as material saturation changes. There further appears to be a constant liquid gradient between the upper and lower regions of the sample. This liquid uptake relationship mirrors what was seen when considering liquid uptake within a fully submerged sample discussed with reference to Figure 6.4.

The samples within the experimental rig are measured to be at a bulk lower liquid content of $0.7g\frac{g_{liq}}{g_{drysample}}$ when compared to an equivalent of up to $1.3g\frac{g_{liq}}{g_{drysample}}$ for the fully submerged sample.this distinction is due to with the smaller liquid contact area within the experimental rig. It is further known, as visualised in Figure 5.4, that the fibre orientation is very biased towards fibres laying in the longitudinal direction rather than the through thickness direction. In this way it can be of great value to isolate the mechanisms responsible for these liquid uptake rates through calculation of the rates liquid diffuses into the through-thickness. This would not only allow for increased understanding of the processes but also be of great value looking at future work on these materials from a simulation viewpoint.

Prior to analysis of this, an interesting phenomenon is noted in the initial liquid transfer; this being the point when the driving force for moisture transport due to concentration differences is highest. It appears to take time to be registered by the MRI as visualised in Figure 6.19. Figure (a) displays a comparison between the signal attained from a dry sample and the recorded signal average over the first 2 minutes for 3 independent material B tests within the 2 minute temporal resolution.

What is clear is the similarity between the signal profiles. Comparing the sig-

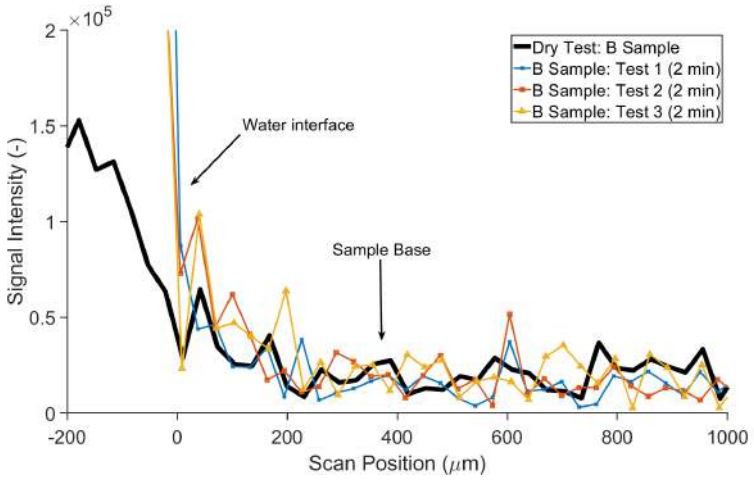


(a) Moisture transport: 2 minutes

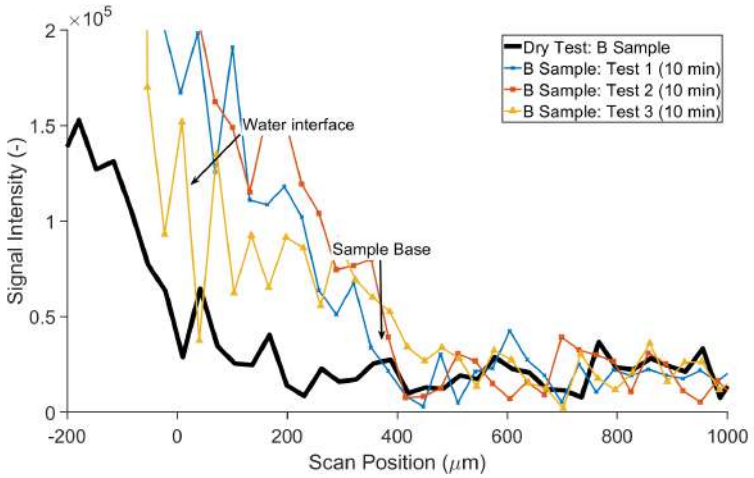


(b) Moisture transport: 10 minutes

**Figure 6.19:** Comparison of moisture transport within a dry Material B sample and 3 independent Material B samples

nal attained after 2 minutes to the signal after 10 minutes seen in the (b) figure is that after 2 minutes there is no increased signal in contrast to the dry sample. Figure (b) is noted to have relatively high noise, notably for test 3; however this is due to the extremely low liquid quantity measurements that are taking place and in a more qualitative than quantitative sense this is not an issue. This lack of moisture transport measured over the first 2 minutes could be due to either the moisture transport not having progressed into the sample through-thickness; the moisture level still being too low to attain signal from or it could be based on the mechanism of moisture transport at play. The MRI, due to the manner in which it operates, attains signal from liquid water and not water vapour. Water vapour is for this reason a possible reason for this phenomena. In 3.2.1 it was discussed how hydrophobized materials are hypothesized to have moisture transport within their structure governed by non-capillary liquid transport. Capillary transport would be characterised by liquid movement within the material and would should be clearly

visible within the MRI signal responses. Vapour diffusion into the fibre pores would however not be picked up by the MRI imaging until it had been absorbed into the fibre structures or adsorbed onto its surface.

Figure 6.20 displays the progression of liquid through the material through thickness during the first 60 minutes.

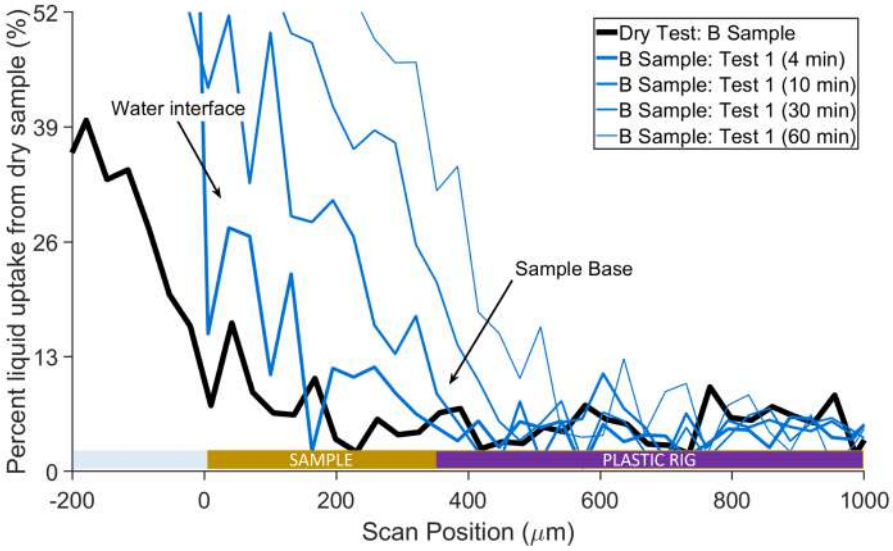


**Figure 6.20:** Translation of liquid progression within the sample B's through-thickness from MRI signal as compared to the total liquid uptake over the 8 hours of testing

What is seen here does not support a hypothesis of initial transport being dominated by vapour transport which then gets absorbed into the fibre structure at which point the liquid would be registered by the MRI. This moisture transport, due to the expected vapour transport rate through the pores commonly expected to be in the range of $10^{-6}m^2/s$, would due to the time-scale enter the fibre not evidently from a certain face on which the moisture makes contact but rather in a more homogeneous fashion. The increase in moisture concentration would thus not expected to be a progressive gradient in the through thickness direction as as appears in the figure but a homogeneous increase. The likelihood of the moisture transport's dominating mechanism for this reason falls more pertinently to diffusion through fibres themselves. Diffusion through the fibre pores is commonly accepted to be a mechanism with a diffusion rate in the range of $10^{-12}m^2/s$.

The progression rate of liquid as it enters the material structure would again be an interesting aspect to distinguish between these different mechanisms. Assessment of the possible diffusion rate within the fibre can add confirmatory weight to the fibre diffusion mechanism playing an important role in explaining the observed moisture sorption dynamics. Calculation of the diffusion rate through the paper's through-thickness is conducted by correlating signal intensities with moisture con-

tents by weight fraction allowing for calculation of the actual diffusion rate.

Initial and final moisture contents after 8 hours of testing of around 0.08g and 0.71g liquid per gram dry material are measured. This indicating a basis from which estimation as to diffusion rates can be calculated. Using this initial approximation as to the initial and final moisture contents is primarily to determine the order of magnitude of diffusion rates as the nature of different mechanism transport rates are within different estimated orders of magnitude.

If moisture transport is split into two separate regimes as per the initial rapid and latter slower liquid uptake regions seen represented and discussed in Figure 6.18, it is appropriate to consider these diffusion rates within the first 20 minutes and after the rate transition independently. In contrast to Figure 6.18 however, the first assessments of diffusion rate are presented without normalisation of the upper limit of the liquid uptake and thus rather with reference to the liquid uptake graph as per Figure 6.21. Here each curve represents a single point through the sample's thickness from the sample surface in black successively to the sample base in light blue. It is important to note that in this case the upper limit is not normalised as in this case it is not a general scale comparison and loose dynamic region analysis that is being considered as was done before but rather a more probing rate analysis upon individual experiments. Figure 6.22 gives the rate of diffusion through material B's through-thickness for these two segments of the moisture uptake.

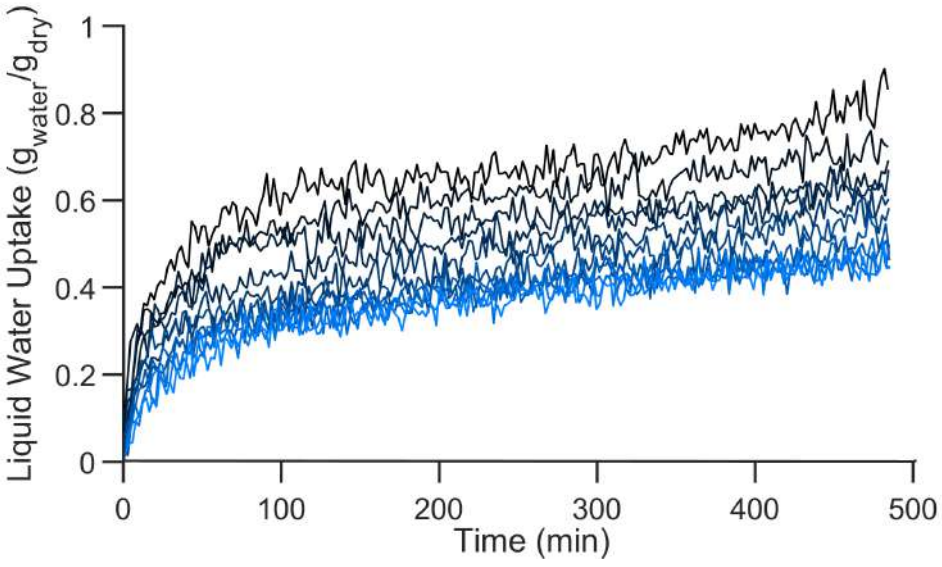


**Figure 6.21:** Moisture uptake of material B test 1 without scaling of the upper liquid content extending from black at the liquid surface to progressively lighter blue towards the sample base.

Diffusion can be calculated using the following function:

$$z^2 = 2Dt \tag{6.1}$$

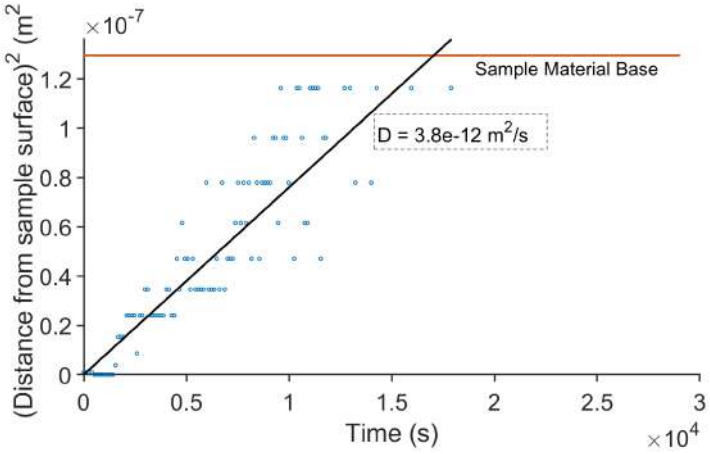


(a) Diffusion rate: initial uptake

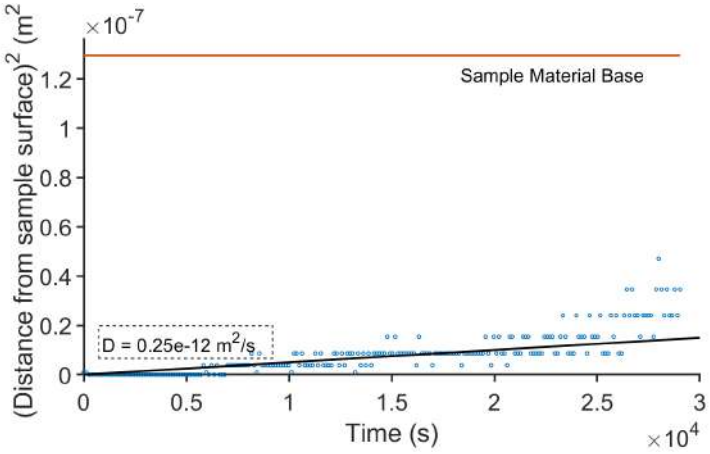


(b) Diffusion rate: latter uptake

**Figure 6.22:** Calculated approximate effective diffusion rate of liquid through sample B's through-thickness

Here $z$ refers to the distance liquid has travelled through the material, $D$ is the diffusion coefficient and t is the time taken to reach the respective reference uptake level. This methodology makes the assumption that the liquid uptake is driven by Fick's law driven by the gradient of moisture per dry sample mass. The assumption is further made that liquid uptake is a function only of time rather than additionally a function of saturation which is likely an oversimplification of the system however for the purposes of this analysis, a feasible approximation. In the case of the initial uptake rate, based off of 6.18, a liquid content per dry sample mass of 0.35g/g is considered an effective reference from which to base the initial diffusion rate as this marks the initiation of the transition point between the two segments. An uptake limit of 0.6 is taken after the transition for the latter mechanism.

The order of magnitude of the diffusion rate is evident as $\times 10^{-12}$ which corresponds well to the fibre diffusion mechanism regime ([3, pg. 31, 33] and contained sources). This valuable outcome can be of great importance when further work in

simulation of moisture transport through material is conducted as a more appropriate weightings and rate descriptions can be given to this mechanism.

This assessment is however not to suggest that there is no moisture transport through vapour which gets absorbed into the fibres. This moisture transport most likely exists but is however, for the contexts of the sample material being in direct contact with liquid water, not considered the dominant mechanism.

### 6.3.4 Uncoated vs coated material comparison

Liquid uptake in coated B2 material and uncoated B is differentiated by B2's 'clay-type' coating for printing visible in comparison between Figures 5.4 and 5.5 which is a porous and hydrophilic layer only micrometers thick that is not hydophobized as are the two pulp types making up the paper material. Comparisons are made between the shorter term liquid uptake rates and extents as well as compared to longer term absorption until the sample nears saturation.

Within the 8 hours of testing, the coated material B2 was found to consistently take up less moisture by mass than the uncoated material B. To the best knowledge of the material's source (Tetra Pak®), the materials are the exact same composition and structure barring the coating layer. The coated B2 however consistently took up $0.6\frac{g_{liq}}{g_{drysample}}$ as compared to $0.71\frac{g_{liq}}{g_{drysample}}$ for uncoated material B. This indicates that the clay type coating does have an impact on liquid uptake. The coating is hydrophilic (designed for ink absorption) and thus uptake within this very thin layer is expected to be high as is seen in Figure 6.23 where a 2D image of material B and material B2 is seen from the top view of the Cobb type experimental rig setup. The white in the image represents the square hole in the rig allowing for the square liquid contact area on the sample surfaces. What is seen is the difference between the signal response of the coated and uncoated material after a long uptake period surrounding the central liquid contact surface being the presence of signal response evidently stemming from the saturated coating that does not appear on the uncoated material. This is visualised by the gray/white texture around the central square present in coated material B2's Figure (b) that is not present in uncoated material B's Figure (a). This suggests a potentially higher lateral movement of liquid radially from the liquid contact area on the liquid surface visible within the coated material.

This phenomenon is not seen exclusively for the coated material B2 as a small fraction of uncoated material B tests appear to show a similar albeit lesser trait; however the consistency of the presence of this is for coated B2 does add weight to the probability of it being due to lateral liquid transport. Potential exists that this difference could be due to a lower sealing effectiveness between the coating and the rubber seal, however the manner in which the coating smooths the material surface as well as the consistency of the sample rig preparation does reduce the likelihood of this being the case.

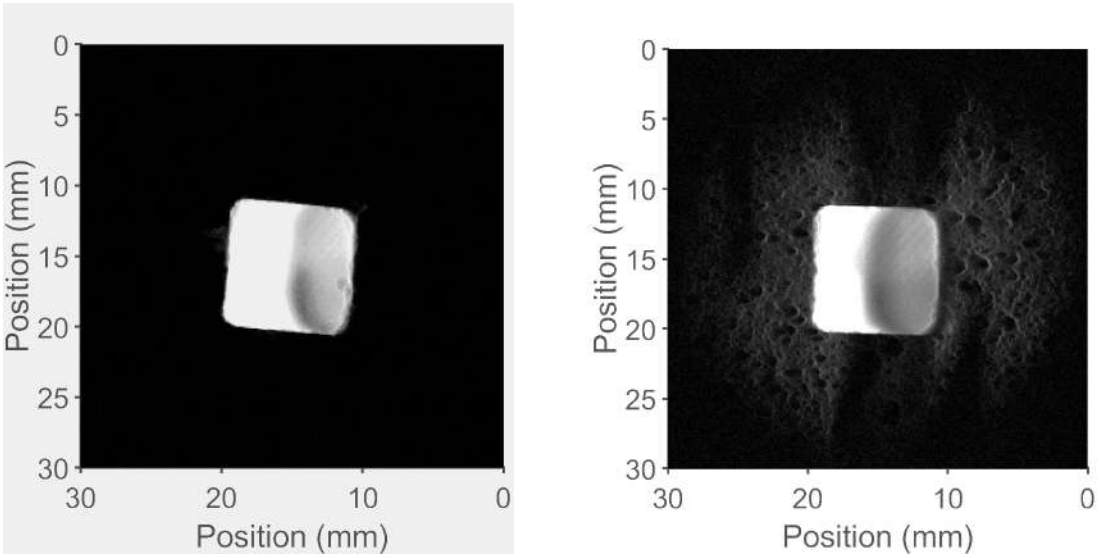


(a) Uncoated material B

(b) Coated material B2

**Figure 6.23:** Visualisation of the coated surfaces liquid uptake as seen from a top down MRI image of the Cobb rig after 8hr testing cycles

The effect on the first faster absorption period is displayed in Figure 6.24. Coated material B2 appears to uptake liquid at a higher rate than uncoated material B. A difference in uptake rate, considering only orders of magnitude, of order difference 1 could be considered significant.

Doubt is however shed on these results due to the effect that scaling and experimental discrepancies have on the result outputs. In these calculations only scaling of the initial moisture content was conducted and not the scaling of the upper limit of the liquid uptake. This thus does not make the assumption that the paper material is saturated across the entire through thickness but rather measurement outputs appear to indicate the presence of a lingering concentration gradient through the material even after over 8 hours of direct liquid contact. It cannot be determined whether this is a representative measurement artefact, a measurement anomaly due to the influence of radial transport into the material sample area not in direct contact with the middle contact square of the experimental rig or simply a manifestation of experimental error. This conclusion cannot be made due to a lack of consistency between tests conducted upon the same material.

As a visualisation of this experimental difference, Figure 6.25 indicates a liquid concentration gradient from the material base (blue) through to the material surface (black) to which the diffusion result of Figure 6.24 (b) describes. This same trend was seen in Figure 6.21 for material B as is described by Figure 6.24 (a). This could however be contrasted to an experimental run within which this long term through-thickness concentration gradient is not apparent, in which case successive points from surface to base through the material thickness different and non-consistent relative liquid uptakes and thus there does not exist a comparative gradient through the

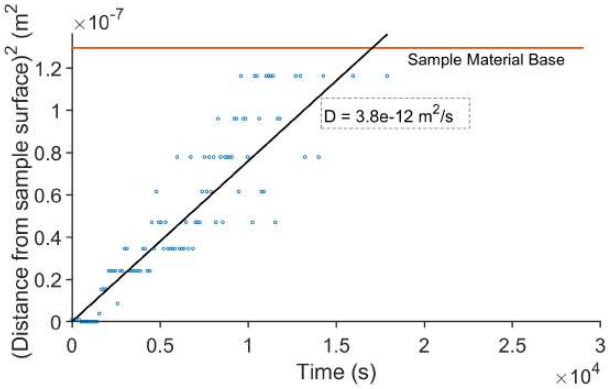


(a) Initial period diffusion rate: Uncoated Material B

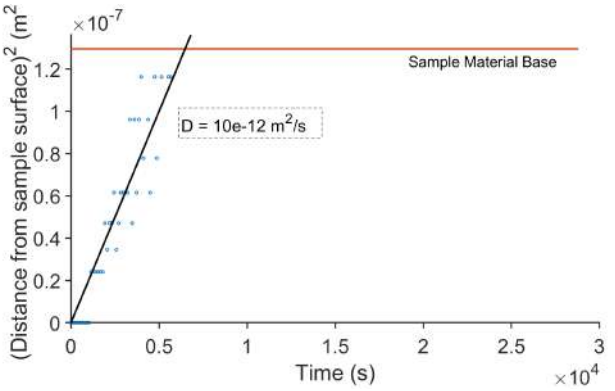


(b) Initial period diffusion rate: Coated Material B2

**Figure 6.24:** Comparison between the diffusion rates of the initial uptake period in coated and uncoated materials B and B2

material.

This alternate gradient in which the higher liquid content at the surface of the sample when compared to through the material thickness is visualised through comparison of two tests, both on material B. Material B test 1 (as described before) compared to material B test 2 displayed in Figure 6.26 (a). Here the base of the sample through thickness (blue) is in fact at a higher liquid concentration than the sample surface. This difference, in contrast to what was seen before in for example material B test 1 does not lead to the ability to confidently prescribe the material diffusion rate as a material property. In the figure (b) the same diffusion co-efficient as measured in material B test 1 is superimposed on the liquid progression through the sample of material B test 2, and conclusive outcomes cannot be drawn due to the lack of a gradient through the material thickness in this specific case.

An absolute difference in the final liquid content is seen between this material B test 1 and test 2 with all tests having a range in final moisture uptakes through the sample thickness of between around 0.4 and 0.8; but through in the same consistent gradient. This described difference is not prescribed as a conclusive outcome of the work, the order of magnitude of diffusion is however put forward as an estimate as to the rate of liquid transport through the material.

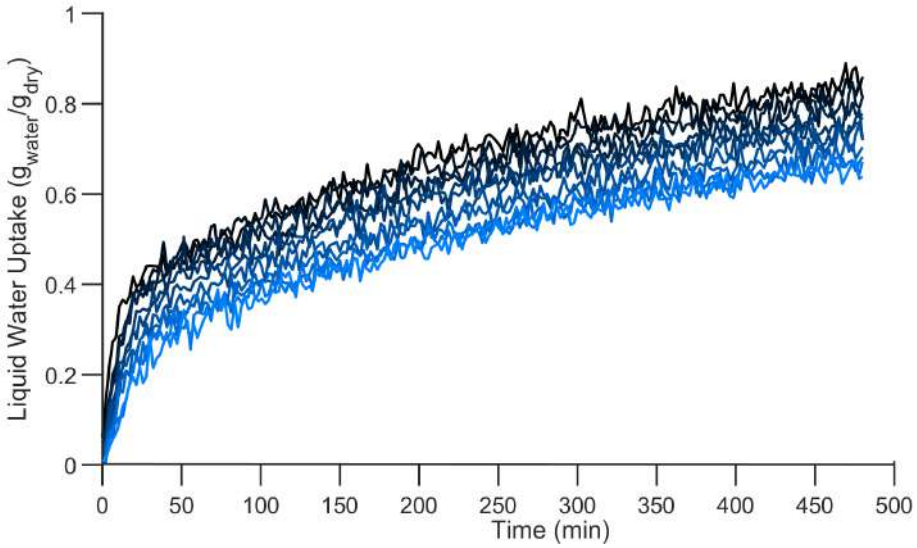


**Figure 6.25:** Moisture uptake of material B2 test 1 without scaling of the upper liquid content extending from black at the liquid surface to progressively lighter blue towards the sample base

The source of the errors which could lead to this difference between tests has been discussed through the results section, ranging from the buckling of the sample material to the implicit operation of the MRI background calculations. Despite these inconsistencies found among the highly dynamic process that is the liquid uptake of natural cellulose based paper fibres, this outcome still represents a significant step forward in the analysis of liquid transport through paper materials on length scales of micrometers.

## 6.4 Application of MRI to study moisture uptake and transport

The MRI has been found to be a tool which lots of potential for usage in characterisation of moisture transport through paper materials in a selection of different contexts through both currently available literature; as well as the expanded applications brought forward through this work. Results attained comprise work conducted in experimental method development for measurement of moisture uptake for hydrophobic materials in an edge-wicking as well as Cobb style testing environment. The novelty of this work is in the application of MRI to moisture uptake from direct liquid contact of a single face at sufficiently high spatial and temporal resolution from an initially dry state to derive mechanistic conclusions as to the moisture transport in the hydrophobic materials.

Work was conducted considering edge-wicking liquid uptake and a method effectively proposed, however not expanded upon further than proof of concept testing

due to the lack of liquid uptake in this context by the hydrophobized materials. A confident estimate for hydrophilic materials as to the temporal resolution of single digit seconds can be proposed for materials thickness 0.6mm and above at a vertical spatial resolution on the order of 50-100$\mu$m while averaging across the entire through thickness of the material. This is expected to be able to be reduced significantly for hydrophilic materials, however optimisation to a further extent than these proposed scales was not conducted during this work. Edge-wicking is however not recommended for hydrophobic materials for which no clear visual edge-wicking is evident.

A Cobb styled testing methodology for either hydrophilic or hydrophobic material has been proposed shown to be functional; with hydrophobic materials being emphasized in finding methodology use as a material characterization technique. In the Cobb style testing setup an emphasis is made on the requirement for incredibly precise test sample positioning due to any minor deviation from ideal positioning reducing significantly the extent to which data analysis can be performed and conclusions be drawn on the data. Samples are recommended to have square liquid contact areas with minimum size of $1cm^2$ with a future work recommendation to explore liquid contact areas of greater than this area. Buckling will always be an issue within this experimental setup over the longer experimental time frames that are able to be considered by MRI imaging. A temporal resolution of 31$\mu$m has been obtained at a temporal resolution of 2 minutes per time-averaged image. This is proposed from the currently available experimental liquid contact area and MRI coil size to be the limit of the temporal and spatial resolution combination. Should the temporal or spatial resolution wish to be improved further then a trade-off between spatial and temporal resolution is required.

It is further not recommended to make use of this Cobb testing methodology for precision focused measurements, but rather relative trend focused measurements. Due to quantitative signal-receivable intricacies based on sample positioning and relative sample/liquid signal quantities as well as the achievable signal-to-noise ratios, trends are able to be attained with a higher degree of confidence and conclusions drawn from such data over time scales in fractions of hours but not to higher detail. Such conclusions drawn to these ends are seen to be applicable in modelling applications where a reference for mathematical characterisations desire a physical reference validation or application baseline from which to draw.

Liquid concentrations below 7% have been confirmed not to be viable for analysis within the MRI at temporal resolutions of 2 minutes or less, and a recommendation is put forward not to consider assessment of liquid of under 10% or even 15% within paper materials should this temporal resolution range be a factor.

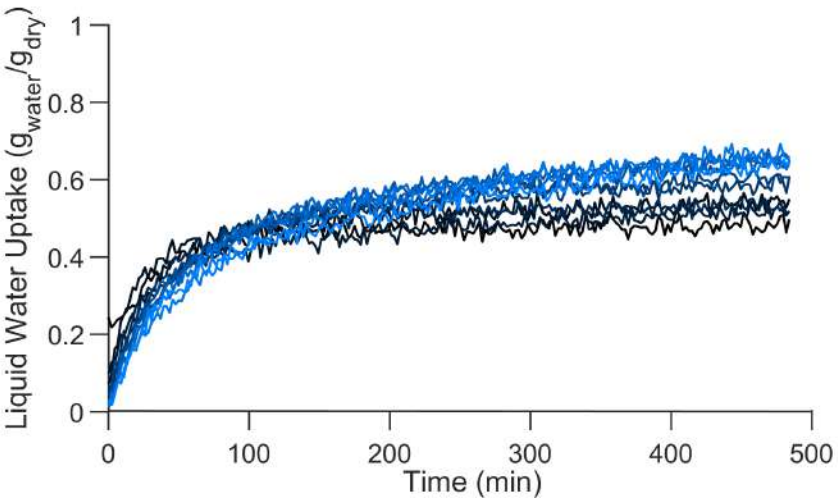


(a) Moisture uptake of material B test 2 without scaling of the upper liquid content extending from black at the liquid surface to progressively lighter blue towards the sample base

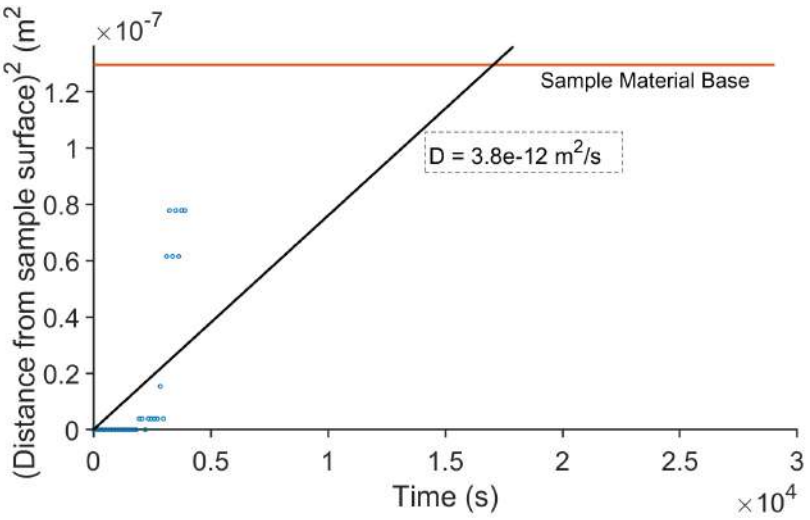


(b) Initial period diffusion rate: Uncoated Material B from test in which the liquid content gradient through the material thickness is inconsistent with prior tests

**Figure 6.26:** Inconsistencies between measured experimental diffusion rates visualised by material B test 2

# 7

# Conclusion and Future Work

The main aim of this study was to to develop a methodology for the measurement of the moisture transport within paper materials using the experimental technique and MRI equipment. This study assessed various testing methodologies to characterise and quantify the liquid transport within paper materials to a high spatial resolution within the MRI.

In this work, the samples tested were of paperboard provided by Tetra Pak® that were sized and had a thickness of 360$\mu$m. The testing procedures explored in this study were in-plane moisture transport (edge-wicking) and through-plane (Cobb styled) tests. The development of these standard tests for the MRI and the optimisation of the MRI parameters for these tests can be followed through in this study. The results obtained comprise mainly of work conducted in the experimental method development for measurement of moisture uptake in the through-thickness direction. An in-plane edge-wicking methodology was effectively developed and proposed, but due to the low liquid uptake by the materials, it is presented primarily as a proof of concept.

This study further analyses the various mechanisms that affect moisture transport within these paper samples within the through-thickness direction using the MRI. Assessing the possible diffusion rate through the paper's through-thickness direction was conducted by correlating the signal intensities received from the MRI with moisture contents by weight fraction, which allows for the calculation of the actual diffusion rate. The order of magnitude of the diffusion rate through the paperboard materials was calculated as $10^{-12}$ $m^2/s$ which corresponds to fibre diffusion regime being the primary transport mechanism. This assessment does not contest presence of moisture transport through vapour as moisture can be taken up into the fibres through vapour, however does not consider it as a dominant mechanism.

This study explored the different issues faced during development of the testing procedures which can lay a good foundation for further work. In particular, isolating the different mechanisms responsible for liquid uptake is very valuable from a simulation point of view with this improved knowledge able to be utilized within computer simulations to predict even faster processes occurring within production of packages or paper straws. This study lays the groundwork for using MRI to successfully study the transport of moisture within paper materials from a perfectly dry state using different testing methodologies.

Further work improving the through-thickness measurement methodology through utilising larger liquid contact areas within the rig could be valuable in increasing the signal-to-noise ratio of the measurements. Making use of a smaller diameter MRI probe to reduce 'dead space' between the coils and measurement zone is a method proposed to explore which could help improve the quality of the signal attained. Further work applying the developed methodologies to different materials, liquids, and temperature ranges will also be valuable in future learning and analysis of materials and liquid uptake studies.

# Bibliography


[1] M. Alexandersson and M. Ristinmaa. "Modelling multiphase transport in deformable cellulose based materials exhibiting internal mass exchange and swelling". In: *International Journal of Engineering Science* 128 (2018), pp. 101–126. ISSN: 00207225. DOI: 10.1016/j.ijengsci.2018.03.013. URL: https://doi.org/10.1016/j.ijengsci.2018.03.013.

[2] M. Alexandersson and M. Ristinmaa. "Multiphase transport model of swelling cellulose based materials with variable hydrophobicity". In: *International Journal of Engineering Science* 141 (Aug. 2019), pp. 112–140. ISSN: 00207225. DOI: 10.1016/j.ijengsci.2019.05.010.

[3] Marcus. Alexandersson. "Macroscopic modelling of coupled multiphysics in swelling cellulose based materials". PhD thesis. Lunds universitet, 2020. ISBN: 9789178955312.

[4] H. Aslannejad and S. M. Hassanizadeh. "Study of Hydraulic Properties of Uncoated Paper: Image Analysis and Pore-Scale Modeling". In: *Transport in Porous Media* 120.1 (Oct. 2017), pp. 67–81. ISSN: 15731634. DOI: 10.1007/s11242-017-0909-x.

[5] A. Bandyopadhyay et al. "Moisture sorption response of paper subjected to ramp humidity changes: Modeling and experiments". In: *Industrial and Engineering Chemistry Research* 39.1 (2000), pp. 219–226. ISSN: 08885885. DOI: 10.1021/ie990279w.

[6] P Bernada, S Stenstro, and S Mansson. "Experimental Study of the Moisture Distribution Inside a Pulp Sheet Using MRI. Part II: Drying Experiments". In: 24.12 (1998).

[7] P Bernada, S Stenstrom, and S Mansson. "Experimental Study of the Moisture Distribution Inside a Pulp Sheet Using MRI. Part I: Principles of the MRI Technique". In: *Journal of Pulp and Paper Science* 24.12 (1998).

[8] Sooyoung Chang and Wonjung Kim. "Dynamics of water imbibition through paper with swelling". In: *Journal of Fluid Mechanics* (2020). ISSN: 14697645. DOI: 10.1017/jfm.2020.219.

[9] R Field. "The Transudation of Water into Paper". PhD thesis. Manchester: Victoria University of Manchester, Nov. 1973.

[10] R George et al. *Resolution and Image Quality*. URL: https://mrimaster.com/about%20us.html.

[11] Sally G Harding et al. *Water transport during the drying of cardboard studied by NMR imaging and diffusion techniques*. Tech. rep. 2001, pp. 5269–5281. URL: www.elsevier.com/locate/ces.

[12] Joseph Hornak. *The Basics of MRI*. Online. Henrietta, NY: Interactive Learning Software, 2012. URL: http://www.cis.rit.edu/htbooks/mri/..

[13] Johannes Leisen et al. "In-plane moisture transport in paper detected by magnetic resonance imaging". In: *Drying Technology* 19.1 (2001), pp. 199–206. ISSN: 07373937. DOI: 10.1081/DRT-100001361.

[14] Johannes Leisen et al. "Through-plane diffusion of moisture in paper detected by magnetic resonance imaging". In: *Industrial and Engineering Chemistry Research* 41.25 (Dec. 2002), pp. 6555–6565. ISSN: 08885885. DOI: 10.1021/ie0204686.

[15] T.Q. Li, T Klason, and L Ödberg. "Water diffusion in wood pulp cellulose fibres studied by means of the pulsed gradient spin-echo method". In: *Journal of Colloid and Interface Science* 154.2 (1992), pp. 305–315.

[16] Andreas Mark et al. "Multi-scale simulation of paperboard edge wicking using a fiber-resolving virtual paper model". In: *Tappi Journal* 11.6 (June 2012).

[17] L. Nilsson, S. Mansson, and S. Stenstrom. "Measuring moisture gradients in cellulose fibre networks: An application of the magnetic resonance imaging method". In: *Journal of Pulp and Paper Science* 22.2 (1996). ISSN: 08266220.

[18] E. L. Perkins and W. J. Batchelor. "Water interaction in paper cellulose fibres as investigated by NMR pulsed field gradient". In: *Carbohydrate Polymers* 87.1 (Jan. 2012), pp. 361–367. ISSN: 01448617. DOI: 10.1016/j.carbpol.2011.07.065.

[19] Jean-Christophe Perrin et al. "Real time monitoring of the through thickness moisture profile of thin sheets using NMR". In: *Chemical Engineering Science* 251 (2022), p. 117464. ISSN: 00092509. DOI: 10.1016/j.ces.2022.117464.

[20] Raymond John Roberts. *Liquid penetration into paper*. Tech. rep. 2004.

[21] P.J Rock. "T1 relaxation time". In: (Feb. 2021). DOI: https://doi.org/10.53347/rID-6315. URL: https://radiopaedia.org/articles/6315.

[22] P.J. Rock. "T2 relaxation". In: (May 2021). DOI: https://doi.org/10.53347/rID-16494. URL: https://radiopaedia.org/articles/16494.

[23] Pekka Salminen. "Studies of Water Transport in Paper during Short Contact Times". PhD thesis. Abo Akademi, 1998. URL: https://www.researchgate.net/publication/35946579.

[24] Pieter Samyn. "Wetting and hydrophobic modification of cellulose surfaces for paper applications". In: *Journal of Materials Science* 48.19 (2013), pp. 6455–6498. ISSN: 00222461. DOI: 10.1007/s10853-013-7519-y.

[25] Kui Song, Ruijie Huang, and Xiaoling Hu. "Imbibition of newtonian fluids in paper-like materials with the infinitesimal control volume method". In: *Micromachines* 12.11 (Nov. 2021). ISSN: 2072666X. DOI: 10.3390/mi12111391.

[26] Lebo Xu, Jeremy Meyers, and Peter W. Hart. "Impact of fiber structure on edge-wicking of highly-sized paperboard". In: *Tappi Journal* 17.8 (Aug. 2018), pp. 437–443. ISSN: 07341415. DOI: 10.32964/tj17.08.437.

[27] J. Yeung and A. Murphy. "Spatial resolution (MRI)". In: (June 2011). DOI: https://doi.org/10.53347/rID-14054. URL: https://radiopaedia.org/articles/spatial-resolution-mri-2?lang=us.

# A

# Appendix A- MRI testing rig design

## A.1 In-plane testing modifications

The initial rig setup for the edge-wicking tests was 3D-printed and provided by Tetra Pak. As discussed earlier, modifications were made as testing continued on the go to remove stability and positioning errors and to get the most effective setup for testing with the available tools.

The main problem faced with the original rig setup shown in A.1 was the sample stability in the holder. Double sided tape and parafilm were used initially in the sample holder to provide stability as seen in A.2. The parafilm was quickly dismissed since it was not firm enough to keep the sample from swaying during testing. Another issue was the swelling of the sample which would cause it to tilt within the MRI during the test. This initial setup also involved placing the main body directly into the probe of the MRI which was then screwed inside. This was not an efficient or accurate form of testing since the probe had to be removed after every test from the MRI which could affect the signal received and calibration of the MRI and it was also time consuming.

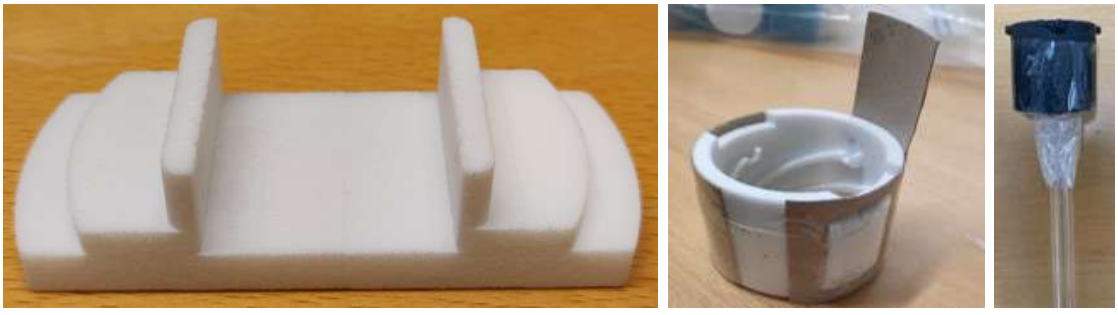

(a) Sample holder (b) Main body (c) Water cup

**Figure A.1:** Initial rig setup

A custom tower was made using empty cardboard paper rolls stacked on top of each other and taped together with the main body of the rig. This worked quite well since the diameter of the main body of the rig was almost the same as the rolls and was able to sit on top of the tower. This modification was made so as to not

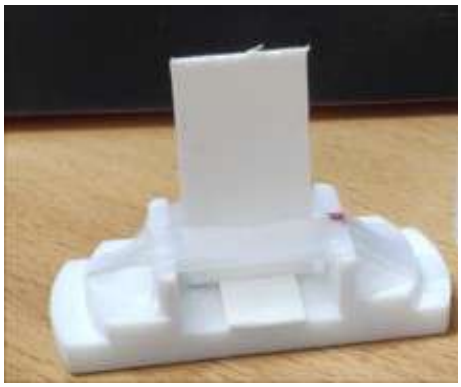

**Figure A.2:** Modification of sample holder using parafilm

**Figure A.3:** Placement of initial rig in MRI probe.

have to remove the probe after every single test. A much sturdier setup would have been preferred but this simple design solved the main purpose for this work.

The initial tests were done on samples that absorb moisture and swell quite rapidly, with the intention being to develop the method of testing before moving on to the commercial paper samples. An issue faced with the double sided tape was that it could not stick to wet samples, so another alternative was considered which is quite similar to prestick. Further testing revealed that the base of the sample that stuck to the holder was not quite as important as supporting it towards the middle. This thought led to 3D printing a new sample holder that had extended wings on the side. The idea was to place a "beam" across the wings and have the sample pass through it. A visual comparison of the old and new sample holder can be seen in A.4.

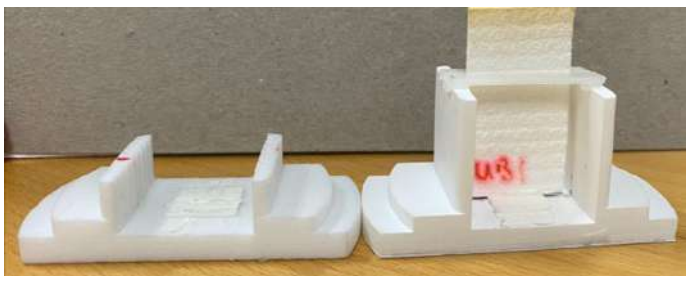

**Figure A.4:** Comparison of old and new sample holder

The new holder proved quite effective for testing and this coupled with the home-made tower made positioning within the MRI much easier. Most of the positioning external to the MRI was done with self-made markings and observations as shown in A.5. This of course is not the most accurate method since human error is a common plausibility when testing. But, overall this testing procedure worked well with the simple adjustments and modifications made.


**Figure A.5:** Positioning of rig inside MRI probe

The final rig deign used involved the new sample holder with the extended wings, the main body which was attached onto the tube of cardboard rolls and then inserted into the MRI probe. The water cup would be inserted right before the measurement was to be taken and all the positioning was done by visible markers and observations. This final rig setup can be seen in 5.8 and 5.9.

## A.2 Through-thickness testing modifications

In order to conduct a Cobb styled test, a paper sample is to lie flat and have free water rest on top of the sample for a certain time period. It is important in this procedure that liquid is not able to enter the sample from it's edge but rather only from the material surface. The goal in this work is to attain the movement of liquid across the through-thickness direction of the paper sample. This requires an extremely high degree of precision.

Initial attempts made use of a rig from Tetra Pak operated from external to the MRI through the use of the same tube utilised for the edge-wicking tests which could be handled from the outside of the MRI machine. A diagram is found in figure A.6. As is seen in the figure, this consisted of a base holder on whose bottom the sample rests that is able to screw into a top-piece that had an O-ring attached which made a seal around the side edges of the circular sample, thereby not allowing liquid to

enter through the sample's edge.

(a) Rig base

(b) Rig top

(c) Complete rig

(d) Rig mounted on tube

**Figure A.6:** Initial rig setup

Results obtained from the use of this external tube did not allow for appropriate representative measurements as variability within the positioning for measurement was unable to be optimised to a degree to which confident predictions and conclusions could be drawn from the result outputs. Figure A.7 is an explanatory exemplar of a test on egg carton material does not allow for accurate definition of where the sample and liquid interfaces are due to bad angling of the sample depsite the large length scales applicable to the test. In this figure it is, due to its thickness and rough surface as well as notably bad positioning, exaggerated when compared to that seen with the sample materials however this exemplar gives a clear indication of how this positioning can hamper data extraction attempts.

Figure A.8 gives a visualisation for this on the more relevant length scales applicable to the material samples.

What can be seen in the figure (a) is a full profile including water positioned above the sample through to measurement below the sample itself. Above the sam-

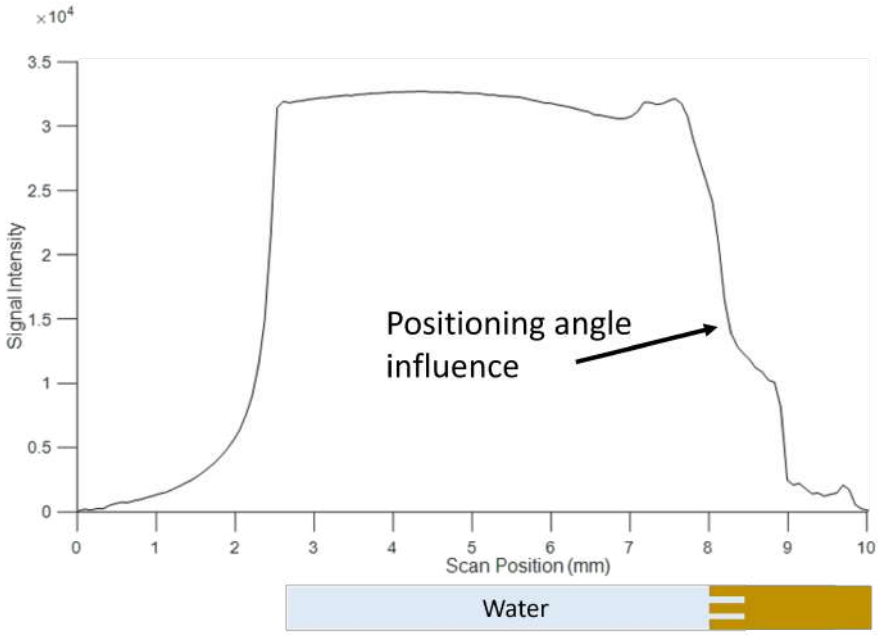


**Figure A.7:** Representative diagram indicating the appropriate orientation of a sample during testing.

ple a high signal intensity is indicative of the free water present above the sample's surface. What is evident is the sheer drop in signal intensity at measurement point scan position 0$\mu$m. At this point the material-liquid interface is found. The plot (b) however indicates the effect that lower accuracy positioning has on the signal attained. It can be seen that the signal sheer drop-off takes place over a distance of 800$\mu$m. The sample itself is however only less than 400$\mu$m thick and the drop-off thus takes place over an area that does not allow for conclusions to be drawn. The nature of insertion of the probe into the measurement area without any ability to confirm positioning before the addition of water means that it, through this result, is not possible to confirm at which point the material face is actually located on the micrometer scale. any conclusions drawn as an experiment runs through time is for this reason prone to error stemming from unknowns. It is not understood whether artefacts and differences in result outputs come from the positioning, from MRI imaging settings chosen or from the sample itself.

The improvements made to the carton material tube base however still did not allow for very accurate measurements due to internal sample positioning factors. These are visible through the selection of plots mounted together in A.9. The figure is representative again of a slice from above the water surface downwards through the entire sample, signal intensity representing the water concentration is high indicating liquid water within the rig for the majority of the plot progressing from the y-axis. Small deviations between position -2000$\mu$m and 0$\mu$m stemming from the shape of rig internals. The curve drop-off following scan position 0$\mu$m represents the liquid-sample interface and further progress through the thickness of the sample. The highest liquid concentration is, due to the circular rubber seal shape, reflective of the material surface. This however only reaches a representative sample liquid

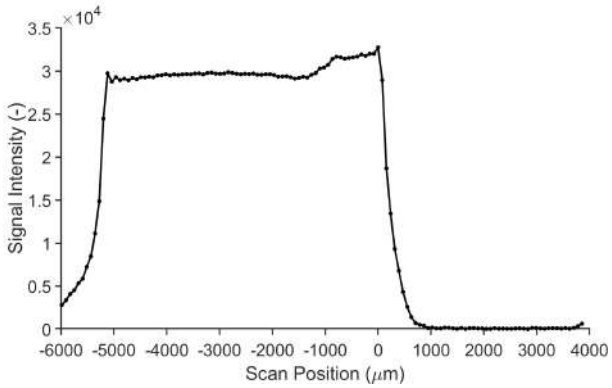


(a) Full field of view signal profile at a single time point

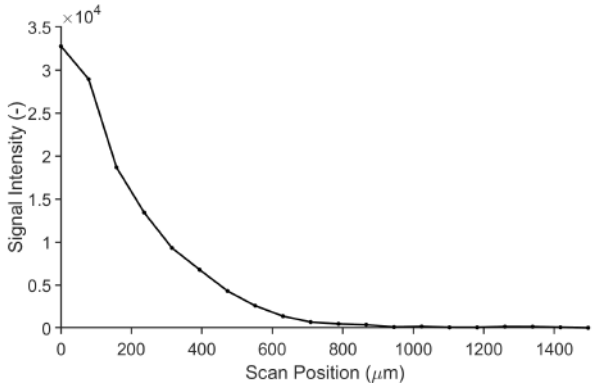


(b) Focused of view signal profile at a single time point

**Figure A.8:** Visualisation of the impact imperfect positioning can have on results analysis and interpretation.

concentration around 500$\mu$m after this point. This downwards curve rather than a precise 'step' change across the interface does not allow for confident assessment of the sample whose thickness is less than 400$\mu$m.

Influencing this error are factors of the measurement area size being too large to be confident of the measurement positioning's stability during testing and the round rubber pressing on the sample possibly distorting measurements. The pressure of the rubber at a localised point on the sample's external boundary compressed the sample in a circle around the edge leading to indents into which liquid water could ingress as seen within the red circled area of A.10. In this figure the white area is representative of liquid within the sample while the black artefacts seen in against the white are rig artefacts as per the figure's explanatory additions. The white area extending down with the round rubber's shadow on the figure's right hand edge is thus the before-mentioned liquid ingress. Furthermore, the flexing of the large inner sample area upwards is visible in the figure. in due to sample having a hole in the middle for visualisation and thus the sample on being visible in the immediate vicinity of the rubber seal.

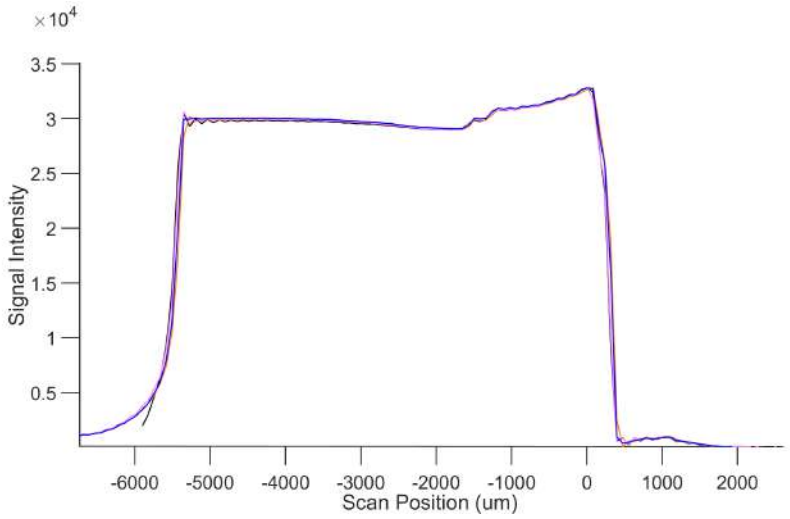


**Figure A.9:** Representative reference curve (with scaled signal intensities) indicating the precision attainable for successive independently set-up experimental runs. This plot consists of 4 stacked experimental runs.

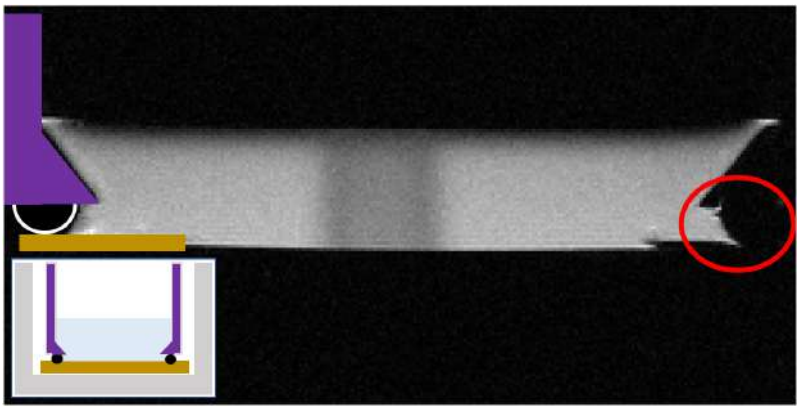

**Figure A.10:** Representative graphic displaying a side profile of the experimental rig as it corresponds to the white liquid water held within the rig. The round rubber and plastic holster with their reference to the sample are visualised upon the left side.

A square alternative to the round rubber seal from before was produced and implemented into the setup. This seal, shown against the rubber ring seal in figure A.11, was however not effective. In addition to this, the effect that the round shape has on the signal profiles was not clearly attainable, however not perceived to be advantageous. For this reason a square sample design was recommended.

**Figure A.11:** Visualization of square rubber seal as compared to the round rubber seal

The first modification made to obtain a square sample surface area was to make circular rubber seal but with a square cutout in the middle. This was made from a simple flexible rubber source and then stuck onto the surface of the sample with a universal contact adhesive (A.12). This method is not recommended as the glue would reacted with the water and formed a type of paste while still allowing there was water leakage to the sides as well. This was however a good proof of concept which led the consturction of a much sturdier seal which is used in the final rig design. Usage of nail polish to paint the surface of the sample and just omit an exposed sample square area unpolished was considered and quickly dismissed. The premise was that the nail polish would act as a barrier between the sample and water and would thus allow water to penetrate only through the square left in the middle of the sample. however the nail polish interaction with water led to the sample getting stuck to the rubber seal and was thus not an effective solution.

**Figure A.12:** Initial rubber seal with square cutout from cycle tube

The most appropriate design was found for reasons summarised before to be that displayed in figure 5.10 reproduced here as A.13. In this design constant pressure on the rubber seal and sample below is maintained by the plastic top-piece. This constant pressure assists in maintenance of the sample's position through the test while the square hole through the rig top-piece and rubber allow for predictable square shaped water-sample contact which can be effectively aligned with the MRI measurement slice. In this way positioning deviations are minimised, the effect of rounded measurement zones are minimised, the possibility for angular errors were before reduced and overall more conclusive artefacts were able to be interpreted

through the design. Through use of this design, more effective results were attained.

Effective measurements conducted using this rig design require MRI imaging optimisation. The methodology and results of this optimisation are presented in B

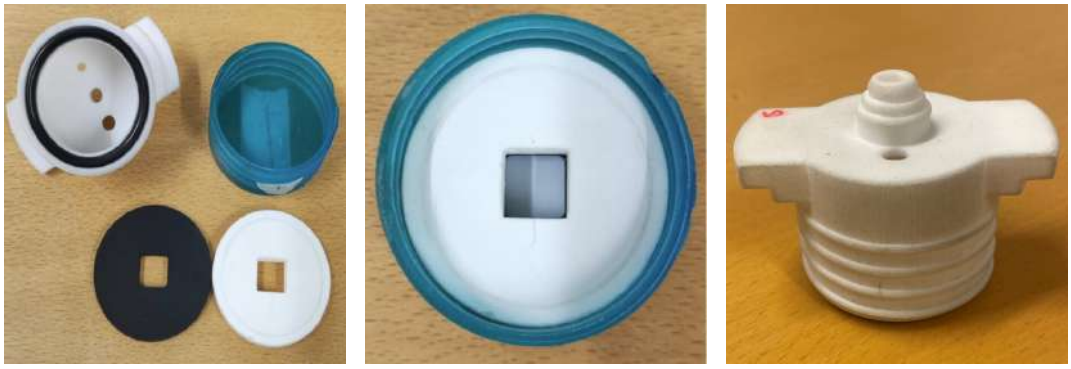

(a) Individual rig units (b) Stacked sealing setup (c) Top support for connection with the sample base

**Figure A.13:** Final Cobb testing rig design

# B

# Appendix B- Final rig MRI settings design and validation

## B.1 Through-thickness testing optimisation

Optimisation of the MRI imaging is essential to successful MRI analysis. The most important parameters to analyse, based on the MRI theory presented in 2.3, are the relaxation time TR, the echo time TE, the field of view FOV, the number of averages as well as the thickness of the measurement slices through the sample.

A field of view of 4mm was chosen based on the proposed relationship that the spatial resolution has with the signal attainable. The lower the spatial resolution- the larger each 1D measurement pixel is and thus the more signal attainable. However due to measurements being conducted on a material's through thicknesses of less than half a millimeter and the desired outcome being the progression of liquid through this thickness; the number of points measured through thick thickness is important. This is a balance between making sure that the resolution is high enough across the full sample and all relevant facets of the rig and sample through thickness are included while maintaining a signal to noise ratio of an appropriate level. Thus having a field of view and hence spatial resolution too large could risk losing details within the sample and having too few independent through-thickness measurement points while having a resolution that is too high could risk having noise negatively impact all results. Table B.1 summarises the potential resolutions of 4 different spatial resolutions at a rig appropriate 4mm field of view.

This is of course interconnected with all other MRI imaging settings and the temporal resolution; though its effect can be visualised independently through fig-

| FOV | Number Points | Pixel Size $\mu$m/point | Points per 360$\mu$m sheet |
|---|---|---|---|
| 4mm | 160 | 25 | 14 |
| | 128 | 31.25 | 11 |
| | 90 | 44.44 | 8 |
| | 48 | 83.33 | 4 |

**Table B.1:** Summary of different field of view properties with a comparison between the resolutions they allow to be attained

ure B.1 where the different spatial resolutions from table are tested using a high number of averages (64) and the most applicable TR and TE times.

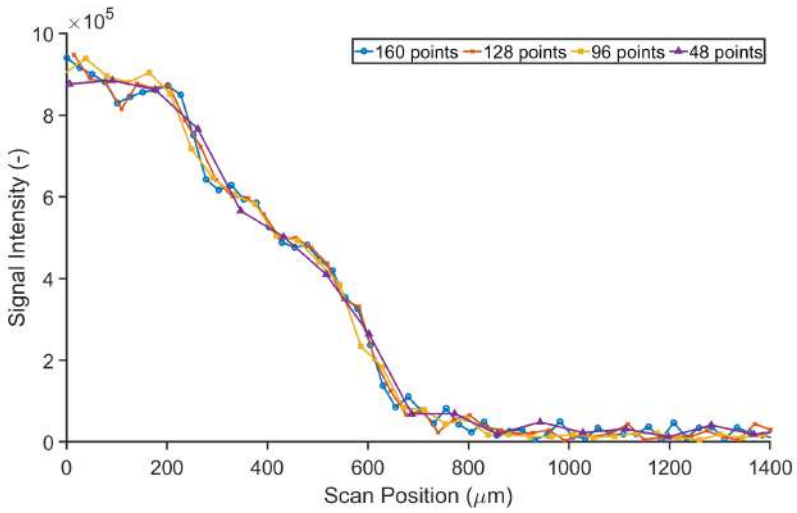


**Figure B.1:** Representative diagram indicating the effect of the field of view on signal intensity received. The largely soaked sample AOI extends from position 0$\mu$m

The initial 4cm FOV proposal was able to be contrasted once further settings optimisations to be summarised below had been conducted as a validation measure for the figure. A lower dependence of the results on the specific spatial resolution chosen in this case within reasonable bounds is seen.

The choice of TR is to a great extent based on the sample's characteristic response within the MRI. During the capturing of an image, the nuclear spin alignments are directionalised by the magnetic field within the MRI and subsequently the response of the spin's decoupling is measured in either the T1 or T2 sense as is in more detail presented and discussed in 2.1. In this work T2 response is focused on most specifically- and for this reason the effect of T1 minimised to the greatest extent possible by minimising TE while the TR time chosen is optimised. Free liquid water and water within the material matrix for this reason have different characteristic responses, and the work requires that the appropriate TR is isolated.

The responses within the sample AOI for different TR values can be shown through figure B.2. In the figure testing of the TR's influence on signal response comes through successive measurements of the same sample at a point seen as effective saturation after the sample's soaking within the rig for over 60 hours.The tests are conducted using 64 averages and a TE of 6.064ms for a good signal

Figure B.2 indicates the low signal at 1000ms when compared to higher signal values of higher TRs. Higher signal with increasing TR is beneficial for results analysis and can allow for lower SNRs- thus more accurate results. For this reason the balance is to be made between increasing of the experimental image acquisition time and the signal attainable. In this work a TR of 2000ms attains good signal as well

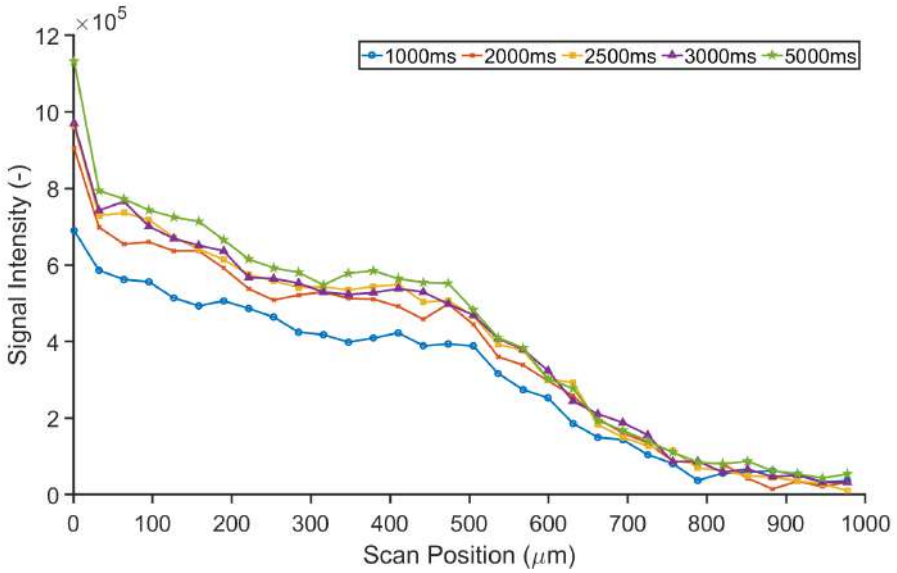


**Figure B.2:** Representative diagram indicating the effect of choice of TR. The largely soaked sample AOI extends from position 50$\mu$m

as a balanced acquisition time and is thus appropriate to use during experimentation.

Slice thickness is a determinant of the amount of signal the MRI scan is able to account for. The larger the sample area over which the through thickness measurement is averaged- the larger the amount of signal able to be considered; with a larger area expected to increase the confidence in the results obtainable through this bulk homogeneous material. Confirmative tests were run at a TR of 2000ms, TE of 6.6524ms and a low number of 8 averages. Figure B.3 visualises and confirms this as the progressively increased signal intensity and thus liquid concentration measured at larger slice thickness. It is to be noted in this figure that the signal to noise ratio is relatively higher- however this is due to the conscious selection of a low number of averages. Furthermore these tests were taken successively from largest to smallest slice thickness on a single sample after 30 minutes of soaking and thus the lower slice thickness' likely had a minutely larger liquid content to measure than the higher- hereby giving more weight to the use of a larger slice thickness. The spatial resolution through which the sample is measured is an additional variable which is to be optimised.

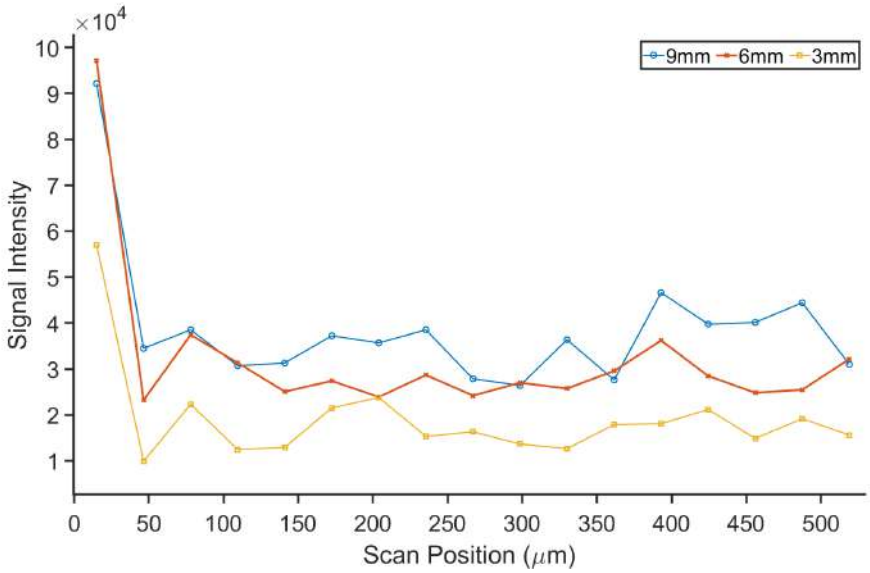


**Figure B.3:** Representative diagram indicating the effect of slice thickness on signal intensity received. The largely soaked sample AOI extends from position 50$\mu$m

**DEPARTMENT OF CHEMISTRY AND CHEMICAL ENGINEERING**
**CHALMERS UNIVERSITY OF TECHNOLOGY**
Gothenburg, Sweden
www.chalmers.se


CHALMERS
UNIVERSITY OF TECHNOLOGY